Title

Structure-function analysis of *Arabidopsis* TOPLESS reveals fundamental conservation of repression mechanisms across eukaryotes

Authors

Alexander R. Leydon[1], Wei Wang[2,†], Hardik P. Gala[1], Sabrina Gilmour[1], Samuel Juarez-Solis[1], Mollye L. Zahler[1], Joseph E. Zemke[1], Ning Zheng[2,3], Jennifer L. Nemhauser[1]

[1]Department of Biology, University of Washington

[2]Department of Pharmacology & [3]Howard Hughes Medical Institute, University of Washington

[†]Present address: Key Laboratory of Plant Stress Biology, State Key Laboratory of Cotton Biology, School of Life Science, Jinming Campus, Henan University, Kaifeng, Henan Province, 475004, PR of China.

Summary

The plant corepressor TOPLESS (TPL) is recruited to a large number of loci that are selectively induced in response to developmental or environmental cues, yet the mechanisms by which it inhibits expression in the absence of these stimuli is poorly understood. Previously, we had used the N-terminus of *Arabidopsis thaliana* TPL to enable repression of a synthetic auxin response circuit in *Saccharomyces cerevisiae* (yeast). Here, we leveraged the yeast system to interrogate the relationship between TPL structure and function, specifically scanning for repression domains. We identified a potent repression domain in Helix 8 located within the CRA domain, which directly interacted with the Mediator middle domain subunits Med21 and Med10. Interactions between TPL and Mediator were required to fully repress transcription in both yeast and plants. In contrast, we found that multimer formation, a conserved feature of many corepressors, had minimal influence on the repression strength of TPL.

Keywords

Corepressors, Transcriptional Repression, Mediator, Tup1, TOPLESS

Introduction

Control over gene expression is essential for life. This is especially evident during development when the switching of genes between active and repressed states drives fate determination. Mutations that interfere with repression lead to or exacerbate numerous cancers (Wong et al., 2014) and cause developmental defects in diverse organisms (Grbavec et al., 1998; Long et al., 2006), yet many questions remain about how cells induce, maintain, and relieve transcriptional repression. Transcriptional repression is controlled in part by a class of proteins known as corepressors that interact with DNA-binding transcription factors and actively recruit repressive machinery. Transcriptional corepressors are found in all eukaryotes and include the animal SMRT (silencing mediator of retinoic acid and thyroid hormone receptor) and NCoR (nuclear receptor corepressor) complexes (Mottis et al., 2013; Oberoi et al., 2011), the yeast Tup1 (Matsumura et al., 2012), and its homologs Drosophila Groucho (Gro) and mammalian transducing-like enhancer (TLE) (Agarwal et al., 2015).

In plants, TOPLESS (TPL), TOPLESS-RELATED (TPR1-4), LEUNIG (LUG) and its homolog (LUH), High Expression of Osmotically responsive genes 15 (HOS15) all act as Gro/TLE-type corepressors (Causier et al., 2012; Lee and Golz, 2012; Liu and Karmarkar, 2008; Long et al., 2006; Zhu et al., 2008). Defects in the TPL family have been linked to aberrant stem cell homeostasis (Busch et al., 2010), organ development (Gonzalez et al., 2015), and hormone signaling (Causier et al., 2012; Kagale et al., 2010), especially the plant hormone auxin (Long et al., 2006). Plant corepressors share a general structure, where at the N-terminus a LIS1 homology (LisH) domain contributes to protein dimerization (Delto et al., 2015; Kim et al., 2004). At the C-terminus, WD40 repeats form beta-propeller structures that are involved in protein-protein interactions (Collins et al., 2019; Liu et al., 2019). In TPL family corepressors, the LisH is followed by a C-terminal to LisH (CTLH) domain that binds transcriptional repressors through an Ethylene-responsive element binding factor-associated Amphiphilic Repression (EAR) motif found in partner proteins (Causier et al., 2012; Kagale et al., 2010). The N-terminal domain also contains a CT11-RanBPM (CRA) domain, which provides a second TPL dimerization interface and stabilizes the LisH domain (Ke et al., 2015; Martin-Arevalillo et al., 2017). While there is speculation that the beta-propellers may control protein interaction with other repressive machinery, it is well-established that they bind to the non-EAR TPL recruitment motifs found in transcriptional regulators (RLFGV- and DLN-type motifs, (Liu et al., 2019)).

We have previously demonstrated the recapitulation of the auxin response pathway in *Saccharomyces cerevisiae* (yeast) by porting individual components of the *Arabidopsis* auxin nuclear response (Pierre-Jerome et al., 2014). In this *Arabidopsis thaliana* Auxin Response Circuit in *Saccharomyces cerevisiae* (*At*ARC^{Sc}), an auxin responsive transcription factor (ARF) binds to a promoter driving a fluorescent reporter. In the absence of auxin, the ARF protein activity is repressed by interaction with a full-length Aux/IAA protein fused to the N-terminal domain of TPL. Upon the addition of auxin, the TPL-IAA fusion protein is targeted for degradation through interaction with a member of the Auxin Signaling F-box protein family (TIR1 or AFB2), and releases the transcriptional repression of the fluorescent reporter. Reporter activation can be quantified after auxin addition by microscopy or flow cytometry (Pierre-Jerome et al., 2014). In the original build and characterization of *At*ARC^{Sc}, it was noted that the two N-terminal truncations of TPL (N100 or N300) behave differently (Pierre-Jerome et al., 2014). While both truncations are able to repress the function of a transcriptional activator fused to an Aux/IAA, only the TPLN100 fusion shows alleviation of repression after auxin addition. TPLN300 fusions to Aux/IAAs maintain strong durable repression even under high concentrations of auxin. This disparity is not due to differential rates of protein degradation, as both proteins appear to be turned over with equal efficiency after auxin addition (Pierre-Jerome et al., 2014).

Structures of the N-terminal domains of TPL rice homolog OsTPR2 (Ke et al., 2015) and the *Arabidopsis* TPL (Martin-Arevalillo et al., 2017) have recently been solved. These structures reveal high conservation of protein folds in the N-terminus, as well as the residues that coordinate formation of homotetramers (Figure 1A). Several lines of evidence suggest that the multimeric TPL modulates repression potential. First, the dominant TPL mutant *tpl-1* altered a single amino acid in the ninth helix of the TPL-N terminus (N176H) that induces aggregation of TPL and its homologs (TPR1-4), reducing total activity (Long et al., 2006; Ma et al., 2017). Second, TPL recruitment motifs found in the rice strigolactone signaling repressor D53 induce higher-order oligomerization of the TPL N-terminus, which increases histone binding and transcriptional repression (Ma et al., 2017). Third, structural studies of *Arabidopsis* TPL demonstrated interdependency of the TPL tetramer formation and Aux/IAA binding (Martin-Arevalillo et al., 2017). One contrary piece of evidence is the strong repressive activity of the TPL N100 construct which lacks the majority of the CRA domain ((Martin-Arevalillo et al., 2017), Figure 1A) and is unlikely able to form tetramers.

The conservation of TPL's repressive function in yeast suggests that the protein partners that enact the repression are conserved across eukaryotes. Consistent with this speculation, the series of alpha-helices that form the N-terminal portion of TPL is highly reminiscent of naturally-occurring truncated forms of mammalian TLE (Gasperowicz and Otto, 2005), such as Amino-terminal Enhancer of Split (AES) (Zhang et al., 2010), the Groucho ortholog LSY-22 (Flowers et al., 2010), and the unrelated mouse repressor protein MXI1 (Schreiber-Agus et al., 1995). Gro/TLE family members are generally considered to repress by recruiting histone deacetylases to control chromatin compaction and availability for transcription (Chen and Courey, 2000; Long et al., 2006). An alternative hypothesis has been described for Tup1 in yeast, where Tup1 blocks the recruitment of RNA Polymerase II (Pol-II) (Wong and Struhl, 2011), possibly through contacts with Mediator complex subunits Med21 or Med3 (Gromöller and Lehming, 2000; Papamichos-Chronakis et al., 2000). However, like many of these family members, multiple repression mechanisms have been described for TPL at different genetic loci. For example, TPL has been found to recruit the repressive CDK8 Mediator complex (Ito et al., 2016), chromatin remodeling enzymes such as Histone Deacetylase 19 (HD19) (Long et al., 2006) and directly bind to histone proteins (Ma et al., 2017).

Here, we leveraged the power of yeast genetics to interrogate the mechanism of TPL repression. Using *At*ARC^{Sc}, we discovered that the N-terminal domain of TPL contains two distinct repression domains that can act independently. We mapped the first, weaker repression domain to the first 18 amino acids of the LisH domain (Helix 1), and the second, more potent domain to Helix 8 which falls within the CRA domain. Full repression by Helix 8 required direct interaction with the Mediator complex, through interactions with Med21 and Med10. This interaction required the same Med21 residues that control transcriptional activation of Tup1-regulated genes in yeast. In addition, we found that multimerization of TPL was not required for repression in yeast or in plants. Our yeast results were validated with plant assays, and extended to include evidence that interaction with the middle domain of Mediator was required for TPL repression of the auxin genes governing lateral root development. Our findings point to a conserved functional connection between Tup1/TPL corepressors and the Mediator complex that together create a repressed state with the capacity for rapid activation.

Results

To understand how TPL represses transcription, we first sought to localize repressive activity within the protein. In the *At*ARC^{Sc}, the extent of auxin-induced turnover of TPLN100 and TPLN300 fusions appear similar, although neither are completely degraded (Pierre-Jerome et al., 2014). One interpretation is that auxin addition increases the sensitivity of the assay to detect subtle differences in the strength of repressive activity of each fusion protein by reducing its relative concentration. In this light, we would argue that TPLN300 is a stronger repressor than TPLN100. To further exploit this synthetic repression assay, we began by generating a deletion series of the N-terminus guided by the available structural information (Figure 1A-B, (Ke et al., 2015; Martin-Arevalillo et al., 2017)). We started with a TPLN188-IAA3 fusion protein construct, which behaves identically to TPLN300 (Figure 1B, (Pierre-Jerome et al., 2014)), and subsequently deleted each alpha helical domain starting with Helix 9 (constructs are named in the format Helix x – Helix y or Hx-Hy). We found that Helix 8 was required for the maximum level of repression activity and for the maintenance of repression after auxin addition (Figure 1C). All constructs lacking Helix 8 retained the ability to repress transcription, but this repression was lifted in the presence of auxin (Figure 1C) as had been observed for the original TPLN100 construct (Pierre-Jerome et al., 2014). Further deletions revealed that including only the 18 amino acids of Helix 1 was sufficient to confer repression (H1, Figure 1D). To test whether Helix 8 activity depended on Helix 1, we tested an additional construct consisting solely of Helix 3 through Helix 9 (H3-H9, Figure 1D). This construct was also able to repress ARF activity, thus demonstrating that both Helix 1 (LisH) and Helix 8 (CRA) can act independently of one another (Figure 1D). To identify the minimal domain needed for Helix 8-based repression, we generated new deletions (Figure 1B,E-F). Helix 8 and the following linker were not sufficient for repression (Figure 1E), and removal of Helix 9 or of the linker between Helix 8 and Helix 9 slightly increased sensitivity to auxin compared to TPLN188 (H1-H8Δ8L, Figure 1F). A deletion that removed both the LisH and Helix 8 repression domains (H3-H7) was only able to weakly repress reporter expression (Figure 1F). Together, these results demonstrate that Helix 1 and Helix 8 could act as repression domains, and that the linker between Helix 8 and Helix 9 (which folds over Helix 1) was required for repression following addition of auxin. Helix 1 alone in the LisH domain was sufficient to act on its own as a modular repression domain. The repressive activity of Helix 8 was only functional in the context of the larger Helix 3-Helix 8 truncation that carries the CTLH domain and a portion of the CRA domain.

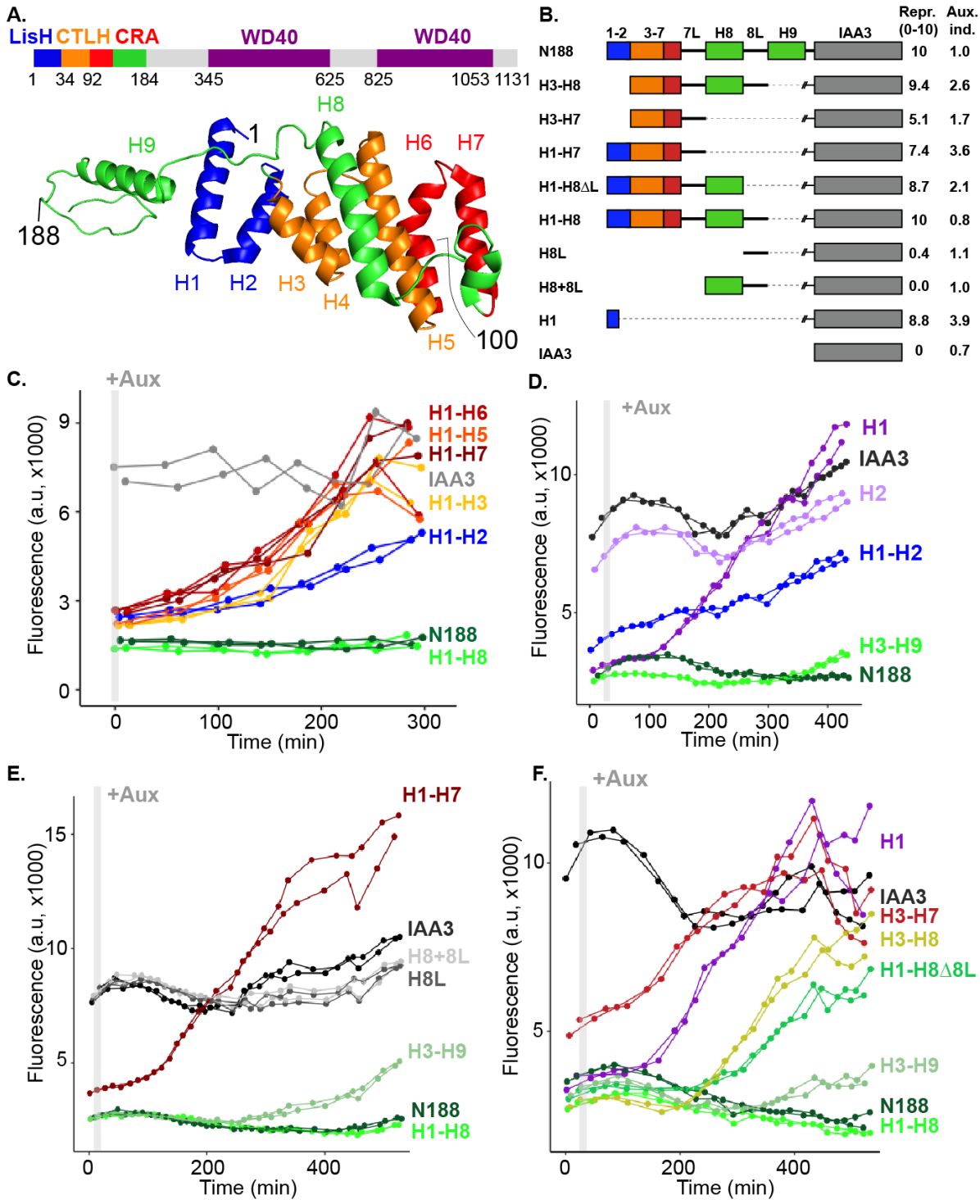

166 **Figure 1. The N-terminal domain of TPL contains two independent repression domains.**

167 **A.** TPL domains are LisH (LIS1 homology motif, blue), CTLH (C-terminal LisH motif, orange),

168 CRA (CT11-RanBPM, red - dimerization and green - foldback), and two WD40, beta-propeller

169 motifs (purple). N-terminal domains are indicated on the solved structure of the first 202 amino

170 acids ((Martin-Arevalillo et al., 2017), 5NQS). The termini of the TPL-N100 truncation used in

171 the original ARC^{Sc} studies is indicated. **B.** Diagram indicating the structure of constructs
172 analyzed in experiments shown in subsequent panels. Repression Index (Rep.) is a scaled
173 measure of repression strength with 0 set to the level of repression observed with IAA3 and 10
174 set to the level of repression by TPLN188-IAA3. Auxin induction level (Aux.) indicates the fold
175 change difference between reporter expression before auxin addition (time zero) and at the end
176 of an experiment (~500 minutes) **C-F.** Helix 1 and the CRA domain (Helix 3-Helix 8) can act
177 independently to repress transcription. Each panel represents two independent time course flow
178 cytometry experiments of the TPL helices indicated, all fused to IAA3. Every point represents
179 the average fluorescence of 5-10,000 individually measured yeast cells (a.u. - arbitrary units).
180 Auxin (IAA-10μM) was added at the indicated time (gray bar, + Aux).
181
182 To determine which of the many known or predicted TPL-binding partners could mediate
183 the repression activity of Helix1 and Helix8, we identified known interactors with either TPL or
184 other Gro/TLE co-repressors, and then introduced the *Arabidopsis* homologs of these genes
185 into the cytoSUS system (Asseck and Grefen, 2018). We chose the cytoSUS system as it would
186 remove the interaction between target proteins to the cytoplasm, as we observed that anchoring
187 the TPL N-terminus had the capacity to repress transcriptional activation of both our synthetic
188 auxin reporter and the activation of yeast two hybrid prototrophy reporters (Figure 1,
189 Supplemental Figure 1A). Putative direct interactors include histone deacetylases (HDACs -
190 AtHDAC9, AtHDAC6, (Long et al., 2006)), Histone proteins (Histone H3, Histone H4, (Ma et al.,
191 2017)), and the Mediator components MED13 (AtMED13, (Ito et al., 2016)) and MED21, which
192 has been demonstrated to interact with Tup1, the yeast homolog of TPL (Gromöller and
193 Lehming, 2000). We did not observe any interactions between TPL-N188 and the HDACs HDA6
194 and HDA9; the histone protein AtHIS4; or the Mediator subunit AtMED13 (Figure 2A,
195 Supplemental Figure 1B). HDAC interaction with TPL has been previously hypothesized to
196 occur through indirect interactions with partner proteins (Krogan et al., 2012), however direct
197 interactions with histones and MED13 have been detected (Ito et al., 2016; Ma et al., 2017). The
198 absence of interaction between TPL-N188 and these proteins may be due to differences
199 between methods, or interaction interfaces in the C-terminal WD40 repeats.
200 Strong interaction was detected between TPL-N188 and AtMED21, a component of the
201 Mediator middle domain (Figure 2A). MED21 is one of the most highly conserved Mediator
202 subunits (Bourbon, 2008), and has a particularly highly conserved N-terminus (Supplemental

Figure 2A,C-E). In yeast, Tup1 interacts with the first 31 amino acids of ScMed21, with the first seven amino acids being absolutely required (Gromöller and Lehming, 2000). We observed that the equivalent truncation of AtMED21 (AtMED21-N31) was sufficient for interaction with TPL-N188 (Figure 2A). We next created truncations of the N-terminal domain of AtMED21 to closely match those that had been made in yeast (Figure 2B, Supplemental Figure 2B) where deletion of the first five amino acids of ScMed21 (ScΔ5Med21) severely reduce the ability of the Mediator complex to co-purify with Pol-II and CDK8 kinase complex (Sato et al., 2016). Interaction between TPLN188 and AtMED21 similarly required the first five amino acids of AtMED21 (Figure 2B), and this truncation did not significantly impact protein levels (Figure 2B).

We used cytoSUS screening to ask whether TPL-N188 interacted with other middle domain Mediator components, and identified an interaction with AtMED10B (Figure 2C). There are two MED10 isoforms in *Arabidopsis*; AtMED10A and AtMED10B with 76.5% amino acid identity between isoforms, and *AtMED10B* is nearly always expressed at a higher level than *AtMED10A* (Klepikova et al., 2016). Consistent with the cytoSUS results, TPLN188 was able to pull down both AtMED21 and AtMED10B from yeast extracts (Figure 2D). AtMED21 interaction was specific to the Helix8-based repression domain, as it interacted with TPLH3-H9 (Figure 2E), and not TPLH1-H5 (Supplemental Figure 1C). A manual juxtaposition of the yeast Mediator structure with the *Arabidopsis* TPL N-terminal structure shows that Helix 8 and 9 of TPL face away from the tetramer, and are therefore optimally placed to interact with Mediator components (Figure 2F).

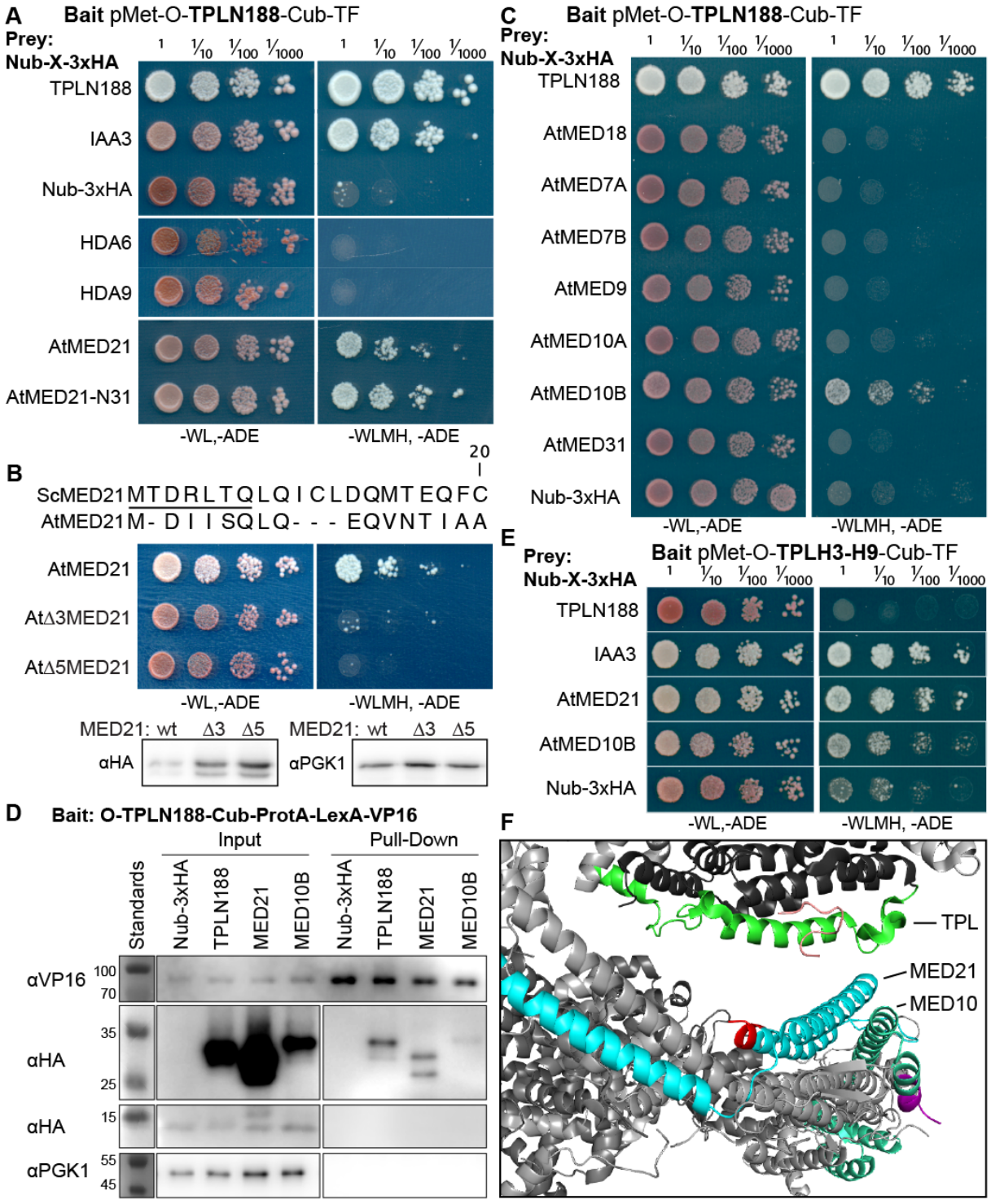

223 **Figure 2. The Helix 8 repression domain of TPL directly interacts with AtMED21 and**
224 **AtMED10B. A-C,E.** cytoSUS assays with candidate interacting proteins. Nub-3xHA is the N-
225 terminal fragment of Ubiquitin expressed with no fusion protein and is used as a negative
226 control. Each prey protein is from *Arabidopsis*. -WL, -ADE - dropout lacking Trp, Leu and Ade

(growth control), -WLMH, -ADE – dropout lacking Trp, Leu, His, Met, and Ade (selective media). **B**. Alignments of the *Arabidopsis* (At) and *Saccharomyces* (Sc) MED21 proteins are shown above cytoSUS assays with the same bait shown in (**A)**. Western blots below the colonies indicated that AtMED21 N-terminal Δ3 and Δ5 are well expressed in assay conditions. **C.** cytoSUS assays with selected Mediator proteins in the middle module. **D.** The TPL-ProteinA-TF fusion protein can pull down TPL, AtMED21 and AtMED10B from yeast extracts using IgG-beads. Detection of the VP16 transcriptional activator demonstrates enrichment of the fusion protein (αVP16). Each prey protein is detected via the 3xHA tag (αHA), and efficacy of purification was judged by PGK1 depletion (αPGK1). **E.** A TPL-N truncation lacking the LisH domain (TPLH2-H9) could still interact with the AtMED21-N31 truncation. This bait construct interacted with IAA3, but only minimally with the negative control (free Nub-3xHA). **F.** Yeast Mediator (bottom, 5N9J) and AtTPL (top, 5NQV) manually docked to compare relative domain sizes and feasibility of a TPL-MED21-MED10B interaction. TPL Helix 8-9 is colored green. MED21 is colored aqua, with the N-terminus colored red, and the EAR peptide in orange. MED10 is colored teal, with the C-terminus colored purple.

To pinpoint which residues of Helix3-9 could coordinate repression through interaction with MED21, we identified likely solution-facing amino acids from Helix 8, as this helix had the greatest impact on repression strength (Figure 1C). We hypothesized that these amino acids were not involved in stabilizing the hydrophobic interactions between intra-TPL helical domains and might be available to interact with partner proteins. In the context of H3-H8-IAA3, eight amino acids in Helix 8 were mutated to alanine (Figure 3A, light green residues). Repression activity was assessed in the absence (Figure 3B) or presence (Figure 3C) of auxin. No single amino acid was essential for repression (Figure 3B). Two mutations (R140A and K148A) slightly increased baseline expression of the reporter (Figure 2B-C). All mutations, except E152A that behaved similarly to controls, altered the stability of repression after auxin addition, either by increasing (S138A,V145A, E146A, K149A) or decreasing (I142A) the final fluorescence level (Figure 2C). Mutating E146 and K149 also increased the speed with which the reporter responded to auxin (Figure 2C), suggesting that these two neighboring residues could be a critical point of contact with co-repressive machinery. S138A had a small increase in auxin sensitivity, while I142 reduced auxin sensitivity (Figure 2E). TPL/TPR corepressors are recruited to transcription factors through an Ethylene-responsive element binding factor-associated

Amphiphilic Repression (EAR) motif (Causier et al., 2012; Kagale et al., 2010), which binds to the TPL in a pocket adjacent to Helix 8 (Ke et al., 2015; Martin-Arevalillo et al., 2017). While these two residues (S138A, I142) do not contact the conserved leucine residues of the EAR motif (LxLxL), in the AtTPL structure, the C-terminal portion of the IAA27 EAR domain makes contact with these residues (Martin-Arevalillo et al., 2017). As we are using a TPL-IAA fusion protein, repression does not depend on EAR-TPL interaction, therefore making it difficult to fully assess any role this interaction normally plays in recruiting repression machinery.

We tested whether the residues in Helix 8 that were required for repression (V145, E146, K148, K149, Figure 3A-C) were also required for interaction with AtMED21. Single alanine mutations of these four amino acids in the context of TPLN188 significantly reduced interaction with AtMED21, while the quadruple mutation (here called Quad^{AAAA}) completely abrogated AtMED21 binding (Figure 3D). These mutations had little effect on interaction with AtMED10B (Supplemental Figure 1D). Additionally, we observed that most of these single mutations decreased binding between TPL and IAA3, consistent with their position along the EAR binding pocket (Figure 3D). When tested in the *At*ARC^{Sc}, TPLN188-Quad^{AAAA} resembled the repressive activity of wild-type N188 (red and black, Figure 3E), consistent with the observation that Helix 1 is present in this construct and is sufficient for repression (Figure 1D). Introduction of Quad^{AAAA} mutations into the Helix 3 through Helix 8 context (H3-H8-Quad^{AAAA}) largely phenocopied a Helix 3 through Helix 7 truncation (H3-H7, Figure 1F) with a drastically reduced repression strength and rapid alleviation of repression by auxin addition (yellow and pink, Figure 4E). Residual repression in H3-H7 likely comes from binding to MED10B, which binds outside amino acids 145-149 (Supplemental Figure 1D). These results indicate that the CRA domain (H3-H8) requires contact with MED21 to repress, and that this is independent of the repression via Helix 1.

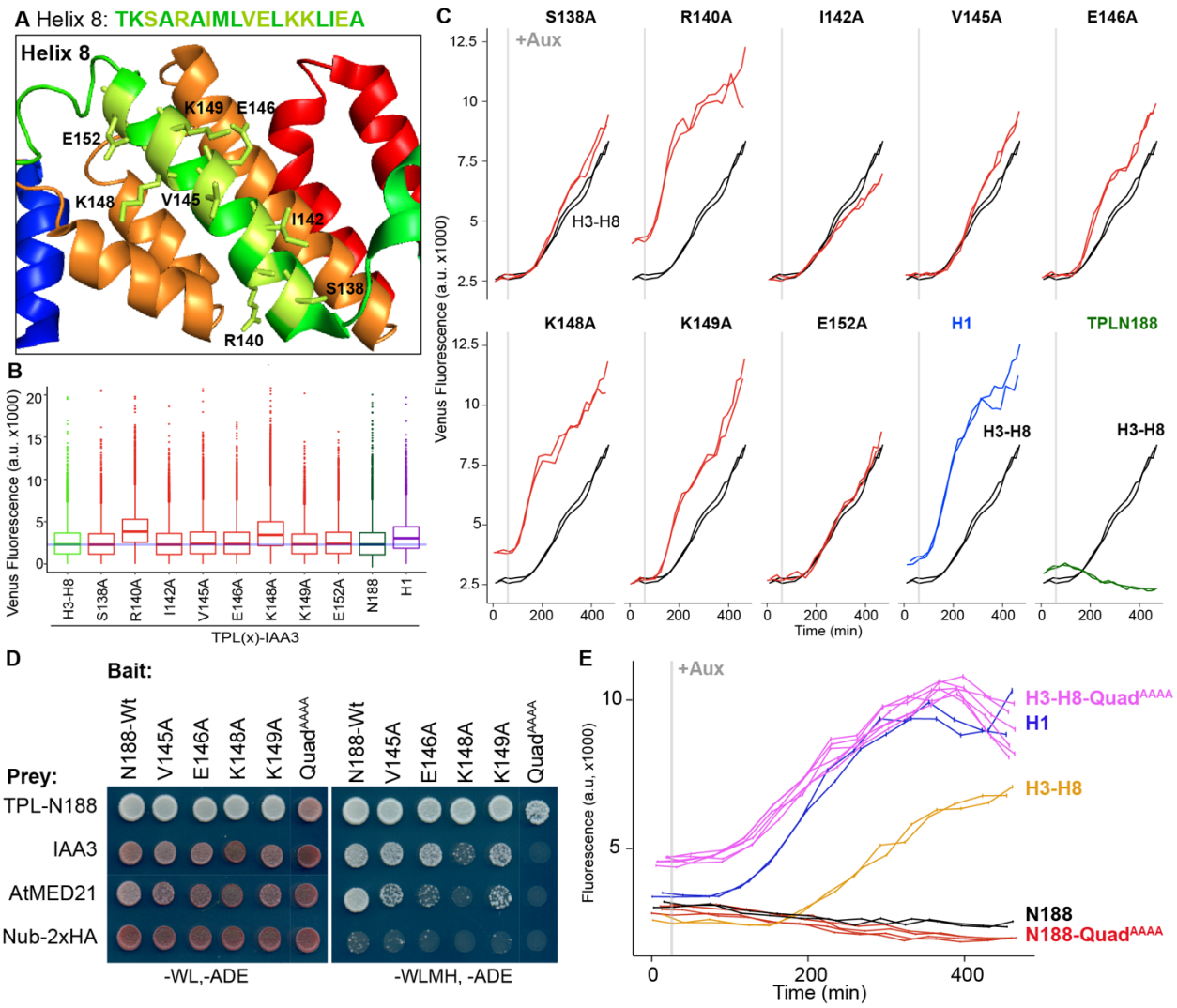

Figure 3. Identification of critical residues within Helix 8 repression domain. A. Sequence and structure of Helix 8 (5NQS). Helix 8 is colored green, and amino acids chosen for mutation are highlighted in light green in both the sequence and the structure. **B.** Repression activity of indicated single and double alanine mutations. **C.** Time course flow cytometry of selected mutations of Helix 8 following auxin addition. TPLH3-8-IAA3 fusion proteins (black) were compared to indicated single mutations to alanine (red). Controls - Helix 1 (H1 – blue), and TPLN188 (dark green). **D.** A series of alanine mutations (V145A, E146A, K148A, K149A, and the quadruple mutant Quad^{AAAA} chosen from Figure 2D-F) were introduced into the TPL-N188 bait construct and tested for interaction with wild-type TPL-N188, IAA3 and AtMED21. Each single alanine mutation reduces TPL interaction with AtMED21, while the quad mutation abrogated interaction. These mutations also reduced the binding strength of TPLN with IAA3. **E.** The Helix 8 Quad^{AAAA} mutation was introduced into the TPLN188-IAA3 and TPLH3-8-IAA3

fusion proteins and compared to wild type N188 in time course flow cytometry. For all cytometry experiments, the indicated TPL construct is fused to IAA3. Every point represents the average fluorescence of 5-10,000 individually measured yeast cells (a.u. - arbitrary units). Auxin (IAA-10μM) was added at the indicated time (gray bar, + Aux). At least two independent experiments are shown for each construct.

The TPL N-terminus (N188) interacted with at least two components of the Mediator complex, AtMED21 and AtMED10B, and interaction between residues in Helix 8 (V145, E146, K148, K149) were necessary for repression (Figure 3). These results suggest that the Mediator complex is required for the TPL N-terminal domain to control repression (Figure 4A). To determine whether a protein-protein interaction is required for corepressor function, it is critical to demonstrate that reciprocal loss of function mutations activate repressed genes. In the case of Tup1, a standard approach has been to test deletion mutations of Tup1-interacting proteins to determine whether their interaction represents a true repression modality on the target gene (Gromöller and Lehming, 2000; Lee et al., 2000; Zhang and Reese, 2004). We sought to test whether loss of function in the Mediator complex would result in activation of the TPL-repressed reporter in the *At*ARC^{Sc}. However, Mediator loss of function mutants can be lethal or exhibit drastic physiological phenotypes (Biddick and Young, 2005). Instead, we combined the Anchor Away system for rapid, chemically conditional protein depletion (Haruki et al., 2008) with the auxin response circuit (Figure 4B).

*At*ARC^{Sc} integrates components at four genomic locations using prototrophic markers that are not compatible with those needed for Anchor Away. To overcome this limitation, we re-recreated the entire ARC on a single plasmid (SLARC) using the Versatile Genetic Assembly System (VEGAS, (Mitchell et al., 2015)). SLARC behaved with similar dynamics to the original *At*ARC^{Sc} on both solid and liquid growth conditions (Supplemental Figure 3A-C). As a first test of the Anchor Away system with SLARC, we fused Tup1 and its partner protein Cyc8 to two copies of the FKBP12-rapamycin-binding (FRB) domain of human mTOR (Haruki et al., 2008). Rapamycin treatment of strains targeting either of these proteins caused no release of repression, providing confirmation that the ARC acts orthogonally to the yeast corepressor (Supplemental Figure 3D).

To test whether Mediator proteins or specific modules were required for TPL repression we introduced the fully repressed SLARC plasmid containing TPLN188 (SLARC^{N188}) into a

library of Anchor Away yeast strains that allow specific depletion of Mediator components (see Figure 4A-B) developed in (Haruki et al., 2008; Petrenko et al., 2017). Upon nuclear depletion of the target genes we saw a striking activation of the auxin reporter when Mediator components from the Tail, Head, and Middle domains were depleted (Figure 4C-E). We observed a less pronounced activation upon depletion of CDK8 (Figure 4F), suggesting that this module plays an ancillary role compared to the core Mediator complex. It is critical to note that Anchor Away of components that are absolutely required for transcriptional activation will show no activation, such as the Tail triple Anchor Away (17,3,15 - Figure 4C) or the RNA Polymerase II (Pol II) Anchor Away (Rpb1 – Figure 4G). These observations support the interpretation that the entire Mediator core (Tail, Head, Middle) is required for robust repression by the TPL N terminus, which is recruited to the middle domain by MED10 and MED21.

Because we have pinpointed TPL N-terminal repression and protein interaction to the specific region of AtMED21 we chose to focus in on this region in the yeast Med21 protein. Deletion of the first 7 amino acids of ScMed21 (Δ7Med21) partially releases genes that are normally repressed by Tup1 into a transcriptionally active state (Gromöller and Lehming, 2000). We hypothesized that TPL repression would also be partially alleviated by such a deletion. ScMed21 is an essential gene, and yeast carrying deletions like Δ7Med21 grow more slowly than the wild type (Gromöller and Lehming, 2000; Hallberg et al., 2006), which itself alters expression levels of reporters. In fact, even a Δ5Med21 yeast mutant has been demonstrated to alter Mediator assembly as the first 5 amino acids of ScMed21 are required for binding of Pol II and the CDK8 kinase module to the Mediator core (Hallberg et al., 2006; Sato et al., 2016).

We introduced SLARCs with different TPL constructs into strains where ScMed21 wild-type or N-terminal deletions were stably expressed and targets of Anchor Away. Strains expressing ScMed21 with or without FRB fusions behaved similarly (Figure 4H, Supplemental Figure 3E-F). We compared the transcriptional output of the fully repressed SLARC^{N188} in MED21 N-terminal mutants lacking the first three, five or seven amino acids. We observed that all three deletions significantly increased the expression of the reporter in SLARC^{N188}, while no mutation increased the SLARC's sensitivity to auxin (Figure 4H, Supplemental Figure 3E-F). As Δ7ScMed21 did not increase reporter expression when compared to Δ5ScMed21 yet did have a noticeable impact on growth, we did not use it in further analyses. Deletions of ScMed21 N-terminal residues had no effect on repression in SLARC^{H1-H5} but they do impair auxin responsive transcriptional activation (Figure 4I), consistent with the role of this region in promoting Pol-II

recruitment (Sato et al., 2016). The fully repressed SLARC^{N188} in Δ3ScMed21 or Δ5ScMed21 mutants showed elevated transcription of the reporter and when depleted demonstrate an increase in reporter activity (Figure 4J), indicating that there is still residual TPLN188-Mediator interaction taking place. Conversion of the first five amino acids of ScMed21 to the corresponding sequence from AtMED21 resulted in an identical repression profile (Supplemental Figure 4E), and had no effect on yeast growth or viability (Supplemental Figure 4F), further highlighting the conservation of this repression mechanism between the two organisms.

The stably expressed N-terminal deletions of ScMed21 likely alter the expression of multiple yeast genes, and this state change could confound our interpretations of the importance of ScMed21 on TPL repression. To minimize the off-target impact of ScMed21 deletions, we introduced estradiol inducible versions of ScMed21 (iScMed21) into the Anchor Away SLARC^{N188} strains (Figure 4B, (McIsaac et al., 2013)). The combination of all three synthetic systems made it possible to rapidly deplete the wild type ScMed21-FRB from the nucleus while simultaneously inducing ScMed21 variants and visualizing the impact on a single auxin-regulated locus. Depletion of nuclear ScMed21 by Rapamycin increased levels of the reporter in all genotypes examined (Figure 4J) while also increasing cell size even in short time-courses, consistent with its essential role in many core pathways (Supplemental Figure 4A, (Gromöller and Lehming, 2000)). When wild-type iScMed21 was induced, there was a rescue of both phenotypes (Figure 4K, black), whereas induction of either Δ3 and Δ5 variants recapitulated the reporter activation seen in the stably expressed mutant versions (Figure 4K, green and blue, Supplemental Figure 4B). iΔ3Med21 was induced and accumulated at a comparable level to wild type Med21, while Δ5 appears to be less stable (Figure 4L-M). In these short time courses, we did not observe the cell size increases observed in the Rapamycin treatments (populations were evenly distributed around a single mean, suggesting we were observing the immediate effects of the Med21 deletions (Supplemental Figure 4C-D)).

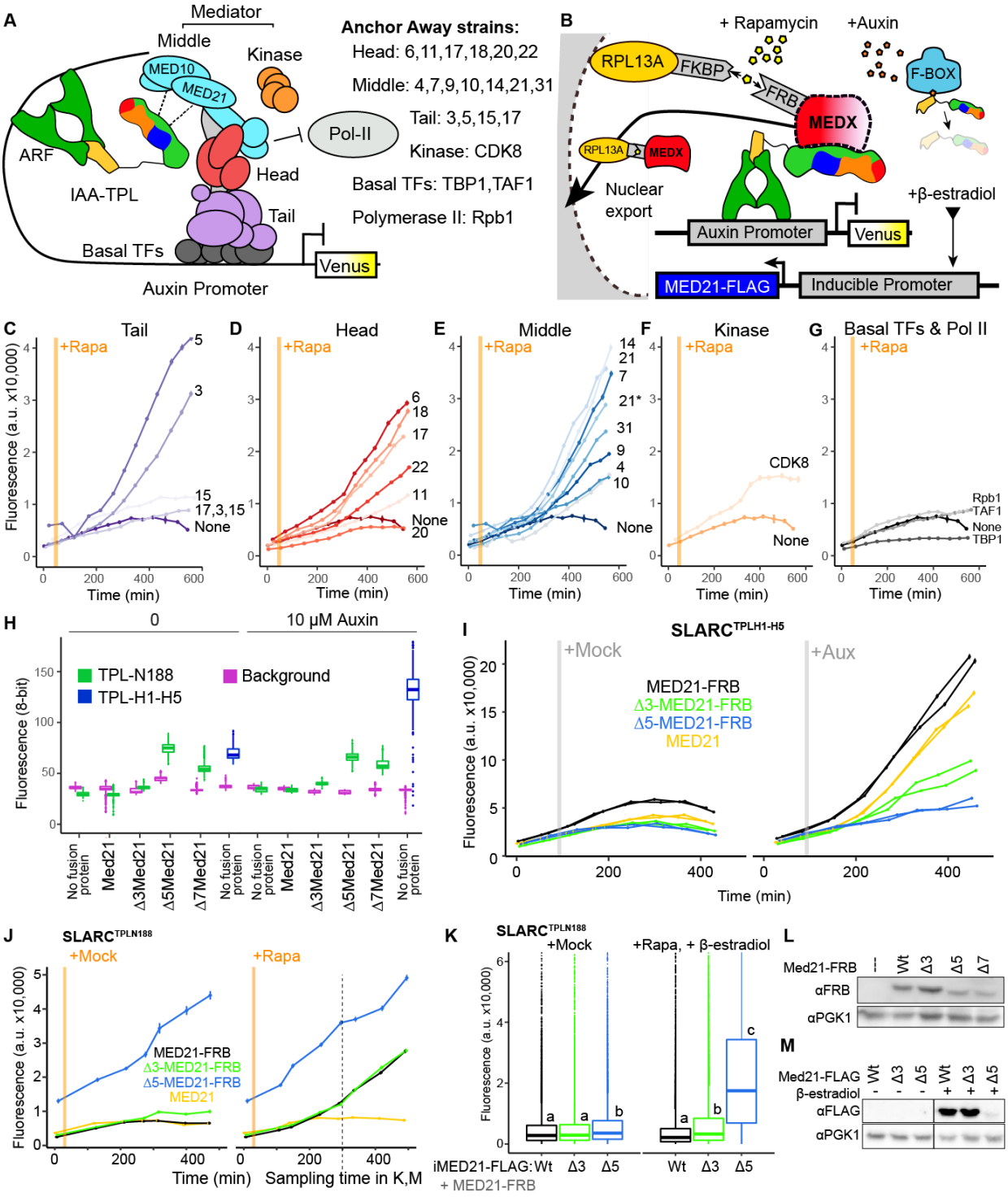

386 **Figure 4. Repression by TPL requires interaction with the N-terminus of MED21.**

387 **A.** Model of the proposed interaction between the TPL N-terminus with Mediator, where TPL

388 interaction with Mediator 21 and 10 inhibit the recruitment of Pol-II. Proteins in this complex that

389 were tested by Anchor Away are listed on the right. **B.** Schematic of *At*ARC^Sc combined with

methods for inducible expression and nuclear depletion of MED21. In Anchor Away, the yeast ribosomal protein 13A (RPL13A) is fused to the rapamycin binding protein FKBP. Addition of Rapamycin induces dimerization between FKBP and any target protein fused to FRB, resulting in removal of the target protein from the nucleus. For these experiments, *At*ARC^{Sc} was assembled into a single plasmid (SLARC) rather than being integrated into separate genomic loci (Figure 4 – Figure Supplement 1). Estradiol-inducible ScMed21 (iMed21) made it possible to replace wild-type MED21 with targeted deletions or mutations. **C-G.** Time-course flow cytometry analysis of SLARC^{N188} in Mediator Anchor Away yeast strains with Rapamycin (orange bar, + Rapa). Two Med21 strains were compared in the Middle domain (E), 21 (generated in this study) and 21* (generated in (Petrenko et al., 2017)). Both 21 and 21* demonstrated similar increases in reporter expression. **H.** Quantification of Venus fluorescence from SLARC^{N188} in wild type and N-terminal ScMed21 deletions with and without auxin. Yeast was grown for 48 hours on SDO media with or without auxin and colony fluorescence was quantified and plotted with the auxin responsive SLARC^{H1-H5} in wild type as a reference. Background - red autofluorescence was used as a reference for total cell density. **I.** Time-course flow cytometry analysis of SLARC^{H1-H5} in wild type and n-terminal ScMed21 deletions with and without auxin. Genotypes are indicated in the colored key inset into the graph. Auxin (IAA-10μM) was added at the indicated time (gray bar, + Aux). **J.** Time-course flow cytometry analysis of SLARC^{N188} in wild type and N-terminal ScMed21 deletions with and without Rapamycin. Genotypes are indicated in the colored key inset into the graph. **K.** Rapid replacement of Med21-FRB with inducible Med21-FLAG demonstrated the requirement for the ScMed21 N-terminus in TPL repression. iMed21 isoforms were induced by addition of β-estradiol (20μM) for 4 hours followed by Rapamycin addition. Fluorescence was quantified by cytometry after 300 minutes (indicated by the dashed box in **D**). Lower case letters indicate significant difference (ANOVA and Tukey HSD multiple comparison test; $p<0.001$). **L-M.** Protein abundance of ScMed21 variants was tested by SDS-PAGE & western blot. For (**C-G, J**) a.u. - arbitrary units. Rapamycin was added at the indicated time (orange bar, + Rapa). Every point represents the average fluorescence of 5-10,000 individually measured yeast cells.

Our data indicated that truncated TPL repression domains were sufficient for interaction with Mediator complex and transcriptional repression, however these truncations (i.e. TPLH3-H8), are unable to form tetramers. This observation re-opened the question as to whether TPL

multimerization affects repression, as both the N-terminus of AtTPL and OsTPR2 adopt a tetrameric form when crystallized (Figure 5A (Ke et al., 2015; Martin-Arevalillo et al., 2017)). We used the cytoplasmic split ubiquitin (cytoSUS) protein-protein interaction assay (Asseck and Grefen, 2018) to test this hypothesis. We observed that Helix 8 was required for strongest interaction between TPL constructs (Supplemental Figure 5A), although this assessment was complicated by the fact that some of the shorter constructs accumulated to significantly lower levels (Supplemental Figure 5B). The weak interaction we could observe between full-length TPL-N and the Helix 1 through Helix 3 construct (H1-3), indicated that the TPL LisH domain is sufficient for dimerization. Therefore, while auxin-insensitive repression may require multimeric TPL, this higher-order complex was not required for auxin-sensitive repression mediated by Helix 1 (Figure 1C-D). In their study of the AtTPL structure, Martin-Arevalillo et al. identified a triple mutation (K102S-T116A-Q117S-E122S) that abrogated the ability of the CRA domain (Helix 6 and Helix 7) to form inter-TPL interactions (Martin-Arevalillo et al., 2017). As this mutant form of TPL is only capable of dimerizing through its LisH domain, we refer to it here as LDimer (Figure 5A). The LDimer mutations in TPLN188 retained the same auxin insensitive repression auxin behavior as wild-type TPLN188 (Figure 5D), supporting the finding from the deletion series.

To make a fully monomeric form of TPL, we introduced mutations into the dimerization interface of the LisH domain in the context of LDimer. We first mutated one of a pair of interacting residues (F15) to a series of amino acids (Tyrosine - Y, Alanine - A, Arginine - R, or Aspartic Acid - D) in the context of either LDimer (Figure 5D), or H1-2 (Figure 5B, 5E). We observed that conversion of F15 to the polar and charged aspartic acid (D) completely abolished repression activity, while the polar and positively charged arginine was better tolerated (Figure 5D,E). The conversion of F15 to tyrosine had no effect on LDimer (Figure 5D), and only a minimal increase in auxin sensitivity in the context of H1-2 (Figure 5E). We then combined LDimer-F15Y with a mutation of the coordinating residue L8 to serine with the intention of stabilizing the now solvent-facing residues. The repressive behavior of this mutant was indistinguishable from that of LDimer (Figure 5F). To further push the LDimer towards a monomeric form, we introduced two additional mutations (S5A, E19S, Figure 5C,G). Size exclusion chromatography confirmed that this combination of mutations (S5A-L8S-F15Y-E19S-K102S-T116A-Q117S-E122S, hereafter called Monomer) successfully shifted the majority of the protein into a monomeric state (Figure 5H); however, this shift had no observable impact on

454 repression strength before or after auxin addition (Figure 5G). To test whether these mutations
455 had a similar impact on *in vivo* TPL complexes, we introduced the LDimer and Monomer
456 mutations into the cytoSUS assay. In contrast to the *in vitro* chromatography results with purified
457 proteins, Monomer expressed in yeast retained measurable interaction with wild-type TPL,
458 LDimer or Monomer, albeit at a reduced level than what was observed between two wild type
459 TPLN188 constructs (Figure 5I). A caveat to this apparent difference between assays is that the
460 Monomer mutations led to a striking increase in protein concentration in yeast (Figure 5 – Figure
461 Supplement 1C), likely partially compensating for the decrease in affinity.
462

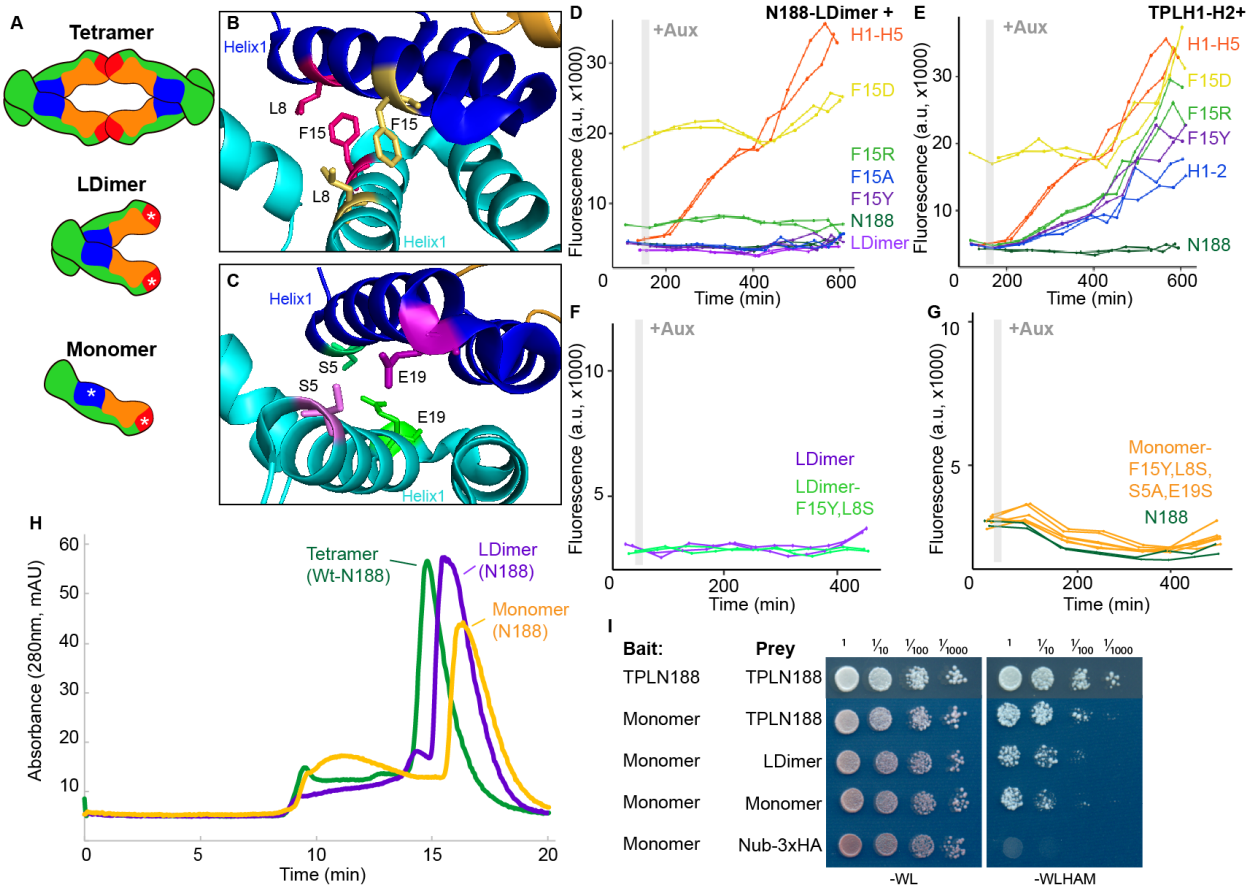

463 **Figure 5. Multimerization is not required for repression in yeast. A.** TPL can form a
464 homotetramer via the CRA (red) and LisH (blue) domains. Asterisks indicate mutations that
465 block or diminish these interactions. **B-C**. Locations of critical positions in Helix 1 are
466 highlighted for two interacting TPL monomers (shown in light and dark blue). Interacting amino
467 acids share the same color (adapted from 5NQV).

D-G. Time course flow cytometry analysis of TPLN-IAA3 fusion proteins carrying selected single point mutations in N188-LDimer-IAA3 (**D**) and the TPLH1-2 truncation (**E**). The F15Y mutation had little effect on repression activity for either TPL construct. Double mutations (F15Y, L8S in LDimer) (**F**) or the quadruple Monomer mutations (S5A, L8S, F15Y, E19S in LDimer) (**G**) showed repression activity that was indistinguishable from LDimer or wild type N188 fused to IAA3. For all cytometry experiments, the indicated TPL construct is fused to IAA3. Every point represents the average fluorescence of 5-10,000 individually measured yeast cells (a.u. - arbitrary units). Auxin (IAA-10μM) was added at the indicated time (gray bar, + Aux). At least two independent experiments are shown for each construct. **H**. Size Exclusion Chromatography on TPLN188 wild type (green), LDimer (purple) and Monomer (orange) tetramerization mutants. **I**. CytoSUS on TPL tetramerization mutants.

While the *At*ARC^{Sc} relies on the strong conservation of the core regulatory machinery in yeast and plants, there are important differences between the synthetic and native systems. For example, while the TPL-N188 construct (and other variants that contain Helix 8 and the linker between Helix 8 and Helix 9) repress transcription in yeast even after auxin addition, this is not the case for the many auxin-regulated genes in plants. To uncover these differences, we first tested for TPL and MED21 interaction using Bimolecular Fluorescence Complementation (BiFC) in *Nicotiana benthamiana* (tobacco). Full-length TPL and MED21 fusions with YFP were localized to the nucleus and did interact with one another by BiFC (Figure 6A). The same TPL Helix 8 residues identified as necessary for a strong interaction with AtMED21 in yeast (Figure 3 - V145A, E146A, K148A, K149A –TPL^{H8QuadA}) were also important for interaction in plants (Figure 6A). Similarly, the Δ5AtMED21 N-terminal truncation completely eliminated interaction with full-length TPL (Figure 6A). Co-immunoprecipitation assays confirmed the AtMED21 and TPL interaction (Figure 6B). We were also able to pull down MED21 and TPL using MED10B from tobacco extracts, supporting our previous interaction assays from yeast (Supplemental Figure 6A).

We next developed a UAS/GAL4-VP16-based (Brand and Perrimon, 1993) conditional, quantitative repression system for plants that relied on induction of a gene encoding a TPLN-IAA14 fusion protein (Figure 6A). To sensitize the output of this assay, we used a variant of IAA14 with mutations in the two EAR domains (EAR^{AAA}) and in the degron (P306S) to block interference from the endogenous TPL/TPRs or auxin-mediated degradation by the TIR1/AFBs,

respectively (IAA14^{mED} ; Figure 6C). After prototyping the system in yeast (Supplemental Figure 6B), we transiently transformed constructs carrying *TPLN-IAA14^{mED}* variants into tobacco to test repression of the well-characterized auxin response promoter DR5 (Ulmasov et al., 1997). DR5 was strongly induced by co-transformation with the transcriptional activator AtARF19. This induction was sharply reduced if the reporter and activator were co-transformed with *UAS-TPLN188-IAA14^{mED}* and *GAL4-VP16* (Figure 6D). In general, we observed strong correlation in repression activity between what was observed in yeast and in tobacco. Truncations containing Helix 1 (H1) or Helix 8 (H3-H9), as well as the full N-terminus (N188), repressed the DR5 reporter (Figure 6D). LDimer and Monomer variants retained a similarly strong repressive activity in tobacco as what had been observed in yeast (Figure 6D). These results are consistent with previous evidence that loss of dimerization through the CRA domain has no effect on transcriptional repression of the DR5 promoter in protoplasts (Martin-Arevalillo et al., 2017). We also observed congruity between yeast and plant data in that the Helix 8 quadruple alanine mutation showed similar repression strength as wild type N188, possibly due to presence of Helix 1 (N188^{H8QuadA} - Figure 6D).

We were concerned that the lack of effect of the Helix 8 mutation and multimerization mutants (LDimer and Monomer) on repression strength could reflect artifacts from heterologous overexpression. To test the effect of these mutants in a native context, we generated transgenic *Arabidopsis* lines where the UAS-TPL-IAA14^{mED} constructs were activated selectively in xylem pole pericycle cells, where IAA14 normally acts to regulate the initiation of lateral root primordia (Figure 6E, (Laplaze et al., 2005)). Transgenic plants expressing functional TPL variants in these cells should make very few if any lateral roots, phenocopying the original solitary root (*slr*) mutant, which carries an auxin-resistant form of IAA14 (Fukaki et al., 2002). As expected, transformants expressing either IAA14^{mED} (with no TPL fusion) or TPLN188 (with no IAA14 fusion) had no effect on lateral root production (Figure 6F). In contrast, TPLN188 fusion constructs sharply decreased lateral root density (Figure 6F). The TPLH3-H9 truncation decreased lateral root density but was not as efficient as TPLN188 stressing the role of the LisH in repression (Figure 6F). Both LDimer and Monomer constructs (Figure 6F) were able to repress lateral root development, meaning that multimer formation is not required for TPL repression of native auxin-induced genes in this context. The fusion containing the Helix 8 quadruple mutant demonstrated a clear loss of repression, indicating that the TPL-MED21 interaction is critical for repression when expressed at endogenous levels (Figure 6F).

AtMED21 loss-of-function mutations are embryo lethal when homozygous (Dhawan et al., 2009; Supplemental Figure 6D), and plants heterozygous for *Atmed21* mutations appear wild-type, including exhibiting normal lateral root density (Supplemental Figure 6E). These phenotypes make testing the specific function of AtMED21interactions with TPL challenging. As an alternative means to probe AtMED21 function in regulating auxin responses, we devised a method to specifically repress transcription of *AtMED21* in xylem pole pericycle cells, similar to the approach used for testing the function of TPL variants. To do this, we introduced a dCAS9-TPLN300 synthetic repressor under the control of a UAS promoter into J0121^{Col-0} along with three sgRNAs complementary to the *AtMED21* promoter. If AtMED21 is required for TPL-based repression, we would expect loss of AtMED21 in xylem pole pericycle cells, which would result in an increase in lateral root number and length. This is indeed what we observed (Figure 6G, Supplemental Figure 6F-G).

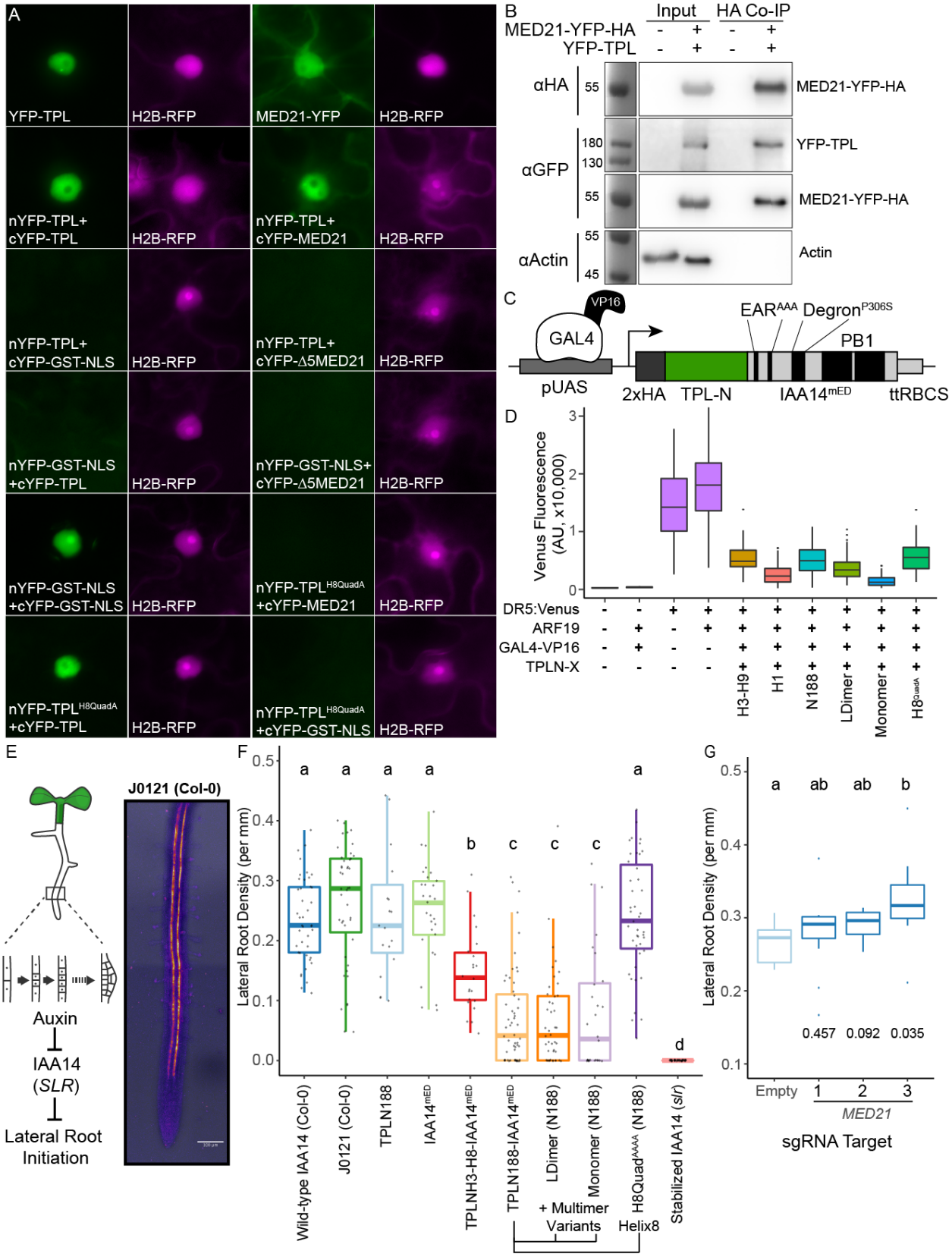

Figure 6. The TPL CRA repression domain behaves similarly in yeast and plants

A. Bimolecular Fluorescence Complementation assay performed in tobacco. Each image is an epi-fluorescent micrograph taken at identical magnification from tobacco epidermal cells at two days post injection. The YFP image is colored green (left panel). p35S:H2B-RFP was used as a control and is false colored magenta (right panel). **B.** Co-immunoprecipitation of MED21 and TPL from tobacco leaves. MED21-YFP-HA was immunoprecipitated using anti-HA, and YFP-TPL was detected using the YFP fusion. Actin was used to demonstrate that the purification had removed non-specific proteins. Numbers on the left of blots indicate sizes of protein standards in kilodaltons. **C.** Design of UAS-TPL-IAA14^{mED} constructs. Mutation of the conserved Lysine residues in the EAR domain disrupted potential interactions with endogenous TPL/TPR proteins. The IAA14 degron has been mutated (P306S) to render it auxin insensitive. UAS – upstream activating sequence, ttRBCS - Rubisco terminator sequence. **D.** Transient expression of indicated TPL constructs in tobacco. DR5:Venus - the synthetic DR5 auxin promoter (Ulmasov et al., 1997) driving Venus, ARF19 - p35S:AtARF19-1xFLAG, GAL4:VP16 - pUBQ10:GAL4-VP16, TPLN-X-UAS-TPL-IAA14^{mED} with various TPL truncations or mutations. **E.** Auxin induced degradation of IAA14 is absolutely required for initiation of lateral root development (cartoon, left). An enhancer trap line (J0121) expresses GAL4-VP16 and UAS-GFP in in xylem pole pericycle cells. **F.** N-terminal domains of TPL were sufficient to repress the development of lateral roots in *Arabidopsis* seedlings. The density of emerged lateral roots was measured in T1 seedlings at 14 days after germination. **G.** MED21-CAS9 repressors targeted to MED21 display increased lateral root densities. Lateral root density (number of lateral roots / primary root length) was calculated at 10 days post germination. Numbers below boxplots are p-values for pairwise comparisons with control using a Wilcoxon rank sum test. **F-G**. Lower case letters indicate significant difference (ANOVA and Tukey HSD multiple comparison test; $p<0.001$).

Discussion

A review of the current literature on corepressors gives the conflicting impressions that (a) corepressor function is broadly conserved, and (b) that every organism (and perhaps even each corepressor) has a distinct mode for transcriptional repression (Adams et al., 2018; Mottis et al., 2013; Perissi et al., 2010; Wong and Struhl, 2011). We hoped that the *At*ARC^{Sc} could facilitate a

578 resolution to this apparent contradiction by targeting repression to a single synthetic locus. We
579 focused our initial efforts on the analysis of the N-terminal portion of TPL which has multiple
580 known protein-protein interaction surfaces (Ke et al., 2015; Martin-Arevalillo et al., 2017).
581 Experiments with the *At*ARC^{Sc} identified two repression domains [Helix 1 and the CRA domain
582 (Figure 1)] within the N-terminus of TPL, both of which were subsequently confirmed to repress
583 transcription in plants as well. This led us to hypothesize that they are therefore likely contact
584 points for other proteins (Figure 2). In the case of the more potent CRA domain, we were able to
585 identify two of these partners MED21 and MED10 (Figure 2). Amino acids within Helix 8 (in the
586 CRA domain) that were critical for repression activity have their R-groups oriented away from
587 the hydrophobic core of TPL structure and are required for Med21-binding and repression
588 (Figure 3). The Mediator subunit Med21 also interacts with the yeast corepressor Tup1, which
589 suggests a fundamental conservation in at least one corepressor mechanism across species.
590 Indeed, the whole core Mediator complex (Head, Middle, Tail) appears to be required for
591 repression through TPL (Figure 4). Contrary to our initial hypothesis, the monomeric form of
592 TPL was sufficient for strong repression in yeast and in plants, leaving open the question of the
593 role of higher-order TPL complex formation (Figure 5). Finally, we were able to show that the
594 TPL-MED21 interaction has functional significance for auxin response in plants (Figure 6).
595 The Mediator complex is a multi-subunit complex that connects DNA-bound transcription
596 factors and the RNA polymerase II complex (Pol-II) to coordinate gene expression (Flanagan et
597 al., 1991; Kim et al., 1994). The yeast Mediator subunits are organized into four separate
598 modules; head, middle, tail and kinase, with a strong conservation of module components in
599 plants (Dolan and Chapple, 2017; Maji et al., 2019; Malik et al., 2017; Samanta and Thakur,
600 2015). Med21 forms a heterodimer with Med7 to and interacts with Med10, among others, to
601 create the central region of the Middle region of the Mediator complex. The Med21 N-terminus
602 is centered on a flexible hinge region (Baumli et al., 2005), which is required for Pol-II
603 recruitment and CDK8 kinase module recruitment (Sato et al., 2016). The protein interaction
604 between TPL and MED21 occurs at the N-terminus of MED21, highlighting the importance of
605 this region as a signaling hub (Sato et al., 2016). Other lines of evidence support this role, as
606 this region binds the yeast homolog of TPL, Tup1 (Gromöller and Lehming, 2000) through a
607 completely different protein domain as no homology can be found between TPL Helix 8 and
608 Tup1 in any region by primary amino acid homology (i.e. BLAST).

Corepressors coordinate multiple mechanisms of repression through discrete protein interactions, leading to robust control over eukaryotic transcription by combining repression modalities. Corepressor function has variously been linked to (a) altering chromatin confirmation, often through interaction with histone modifying proteins or histone proteins themselves, (b) direct interference with transcription factor binding or function and (c) physical spreading of long-range oligomeric corepressor complexes across regions of regulatory DNA (Perissi et al., 2010). Dissection of the importance of each modality in Tup1 repression has been challenging (Lee et al., 2000; Zhang and Reese, 2004). The tour-de-force of corepressor mechanism studies in yeast concluded that the primary function of Tup1 was to physically block activators (Wong and Struhl, 2011). In their work, the authors utilized the Anchor Away approach to correlate the importance of HDACs, transcriptional machinery and chromatin remodeling enzymes to the repression state of endogenously repressed Cyc8-Tup1 target genes. They observed that Tup1 did not block the binding of transcription factors but inhibited the recruitment of one Mediator component in the tail domain, GAL11/MED15, as well as Pol-II and the chromatin remodelers Snf2 and Sth1. They additionally observed that HDACs had only a supportive role in reinforcing Tup1 repression. These results led to their hypothesis that Tup1 blocks the activation domains of transcription factors, and suggested this was through direct binding to activation domains (Wong and Struhl, 2011).

The synthetic system used here allowed us to build on this model and further refine our understanding of TPL's repressive activity. In our experiments we see a similar set of conditions, with TPL recruited to the DNA-bound transcriptional activator (ARF), and several possible mechanisms of repression. Unlike Tup1, we have subdivided the TPL protein to identify interactions between TPL and individual protein interactors with no effect on yeast function. In these experiments we can eliminate the possibility that TPL blocks ARF activation by directly blocking the transcription factor activation domains because we see a loss of repression only when TPL-MED21 binding is eliminated through specific point mutations (Figure 4H). Our inducible swap of MED21 isoforms also corroborates these findings (Figure 4), as the SLARC remains genetically identical in these strains, indicating that TPL-MED21 interaction is regulating activity not a TPL-ARF interaction. Furthermore, our results correlate well with findings that repressed targets are reactivated when this portion of MED21 is deleted in yeast (TPL - Figure 4, Tup1 - (Gromöller and Lehming, 2000)). Therefore, we suggest that instead of directly binding activation domains that TPL (and likely Tup1) binds to components of Mediator

(MED21, MED10B and possibly others) recruited by the transcription factor. Indeed, it is easier to rationalize that the repressor binds the same domains of the Mediator complex recruited by the transcription factor's activation domain (with the same affinity) as opposed to binding each diverse activation domain (with varying affinity). In this model, corepressor binding blocks formation of a fully active Mediator complex thereby limiting Polymerase II recruitment and promoter escape (Petrenko et al., 2017).

Multiple points of contact likely exist between the Mediator complex and other parts of the transcriptional machinery in both transcriptionally repressed and active states. For auxin response, specifically, there are several lines of evidence to support this model, including documented association between the structural backbone of Mediator, MED14, and activated and repressed auxin loci in *Arabidopsis* (Ito et al., 2016). In addition, MED12 and MED13 are required for auxin-responsive gene expression in the root, and MED12 acts upstream of AUX1 in the root growth response to sugar (Raya-González et al., 2018). MED18 in the head module represses auxin signaling and positively regulates the viability of the root meristem (Raya-González et al., 2018). PFT1/MED25 regulates auxin transport and response in the root (Raya-González et al., 2014). MED7, MED21's partner protein in the hinge domain, is required for normal root development and loss of MED7 function impacts expression of auxin signaling components (Kumar et al., 2018). Previous research identified the Mediator CDK8 subunit, specifically MED13 (MAB2), as an interactor with the full-length TPL protein (Ito et al., 2016). We could not observe interaction between the N-terminal domain of TPL and AtMED13, AtCYC8, or AtCYCC (Supplemental Figure 1B), suggesting that any direct interactions occur outside the N188 fragment. As suggested by Ito and colleagues (Ito et al., 2016) and supported by our synthetic system, auxin-induced removal of TPL is sufficient to induce changes in the composition of the Mediator complex, facilitating both rapid activation and rapid return to a repressed basal state.

The conserved interaction of both TPL and Tup1 with Mediator has implications for modeling the dynamics of eukaryotic transcription (e.g., (Estrada et al., 2016)). By stabilizing the Mediator complex, TPL (and by extension Tup1) may create a 'pre-paused' state that allows rapid recruitment of Pol-II and activation once TPL is removed. Alternatively, TPL could allow for recruitment of a poised or paused Pol-II, allowing for rapid activation (and re-activation) of a repressed locus. Support for this idea comes from the genome-wide correlation between Groucho corepressor binding and polymerase pausing in *Drosophila* (Kaul et al., 2014).

673 However, in non-metazoan lineages (i.e. plants and yeast) the existence of bona fide pausing is
674 disputed, mainly due to the absence of the pausing regulator Negative Elongation Factor
675 complex (NELF, (Gaertner and Zeitlinger, 2014)). One possibility is that plants and yeast have
676 an ancestral or alternative form of pausing that is NELF-independent. Support for this idea
677 comes from studies of *Arabidopsis* where Pol-II was found to be markedly enriched at the five-
678 prime ends of genes, the same pattern seen with metazoan pausing (Zhu et al., 2018). In yeast,
679 Tup1 has been implicated in a form of transcriptional memory that involves recruiting a poised
680 form of preinitiation Pol-II to allow rapid reactivation of genes involved in sugar utilization (Sood
681 et al., 2017).
682
683
684 **Methods**
685
686 **Cloning**
687 Construction of TPL-IAA3 and TPL-IAA14 fusion proteins were performed as described in
688 (Pierre-Jerome et al., 2014). Variant and deletion constructs were created using PCR-mediated
689 site-directed mutagenesis. Site-directed mutagenesis primers were designed using
690 NEBasechanger and implemented through Q5® Site-Directed Mutagenesis (NEB, Cat
691 #E0554S). TPL interactor genes were amplified as cDNAs from wild type Col-0 RNA using
692 reverse transcriptase (SuperScript™ IV Reverse Transcriptase, Invitrogen) and gene-specific
693 primers from IDT (Coralville, Iowa), followed by amplification with Q5 polymerase (NEB). These
694 cDNAs were subsequently cloned into Plasmids for cytoSUS using a Gibson approach (Gibson
695 et al., 2009), through the Aquarium Biofabrication facility (Ben Keller et al., 2019). The coding
696 sequence of the genes of interest were confirmed by sequencing (Genewiz; South Plainfield,
697 NJ). For UAS driven constructs, the TPLN188-IAA14 coding sequence was amplified with
698 primers containing engineered BsaI sites and introduced into the pGII backbone with the UAS
699 promoter and RBSC terminator (Siligato et al., 2016) using Golden Gate cloning (Weber et al.,
700 2011). Subsequent mutations were performed on this backbone using PCR-mediated site-
701 directed mutagenesis (see above). Construction of C-terminal 2xFRB fusions for Anchor Away
702 were constructed as described in (Haruki et al., 2008). Inducible MED21 was constructed as
703 described in (McIsaac et al., 2013). For cell type specific knockdown mediated by dCas9-
704 TPLN300, Gibson cloning was used modify the pHEE401E plasmid, replacing the egg-specific

promoter and Cas9 from pHEE401E (Wang et al., 2015) with UAS promoter and dCas9-TPLN300 fusion protein (Khakhar et al., 2018). The resulting plasmid is used as starting point to clone 3 sgRNAs targeting the *AtMED21* promoter (identified using CHOP CHOP (Labun et al., 2019). sgRNAs: GACGCAGAGTCTGTTGGGTGTGG, TTTAAAATGGGCTTTTAAGGTGG, AACACTGAAGTAGAATTGGGTGG ranging from -170 to +90 region from the TSS) using PCR and Golden Gate cloning strategy described in (Wang et al., 2015).

Flow Cytometry

Fluorescence measurements were taken using a Becton Dickinson (BD) special order cytometer with a 514-nm laser exciting fluorescence that is cut off at 525 nm prior to photomultiplier tube collection (BD, Franklin Lakes, NJ). Events were annotated, subset to singlet yeast using the FlowTime R package (Wright et al., 2019). A total of 10,000 - 20,000 events above a 400,000 FSC-H threshold (to exclude debris) were collected for each sample and data exported as FCS 3.0 files for processing using the flowCore R software package and custom R scripts (Supplemental File 1, (Havens et al., 2012; Pierre-Jerome et al., 2017)). Data from at least two independent replicates were combined and plotted in R (ggplots2).

Yeast Methods

Standard yeast drop-out and yeast extract–peptone–dextrose plus adenine (YPAD) media were used, with care taken to use the same batch of synthetic complete (SC) media for related experiments. A standard lithium acetate protocol (Gietz and Woods, 2002) was used for transformations of digested plasmids. All cultures were grown at 30°C with shaking at 220 rpm. Anchor-Away approaches were followed as described in (Haruki et al., 2008), and anchor away strains were obtained from EURO-SCARF (euroscarf.de). Endogenous genomic fusions of ScMed21-FRB were designed by fusing MED21 homology to the pFA6a-FRB-KanMX6 plasmid for chromosomal integration into the parental anchor away strain as in (Petrenko et al., 2017), selectable through G418 resistance (G418, Geneticin, Thermo Fisher Scientific). Tup1-FRB and Cyc8-FRB were constructed as described in (Wong and Struhl, 2011). Mediator anchor away strains were created in (Petrenko et al., 2017) and kindly donated by Dr. Kevin Struhl. SLARC construction required a redesign of promoters and terminators used in the *At*ARC^{Sc} to eliminate any repetitive DNA sequences (See Figure 4 – Figure Supplement 1), using a Golden Gate cloning approach into level 1 vectors. Subsequent assembly of individual transcriptional units

737 into a larger plasmid utilized VEGAS assembly which was performed as described in (Mitchell et
738 al., 2015). To create an acceptor plasmid for the assembled transcriptional units, we
739 synthesized a custom vector containing VA1 and VA2 homology sites for recombination (Twist
740 Bioscience, South San Francisco, CA). In between these sites we incorporated a pLac:mRFP
741 cassette to allow identification of uncut destination plasmid in *E. coli*, flanked by EcoRI sites for
742 linearization. Finally, the CEN6/ARSH4 was transferred from pRG215 (Addgene #64525) into
743 the acceptor plasmid by Golden Gate reaction using designed BsmBI sites engineered into the
744 acceptor plasmid and the primers used to amplify the CEN/ARS (See Figure 4 – Figure
745 Supplement 1). For the cytoplasmic split-ubiquitin protein-protein interaction system, bait and
746 prey constructs were created using the plasmids pMetOYC and pNX32, respectively (Addgene,
747 https://www.addgene.org/Christopher_Grefen/). Interaction between bait and prey proteins were
748 evaluated using a modified version of the split ubiquitin technique (Asseck and Grefen, 2018).
749 After two days of growth on control and selection plates, images were taken using a flatbed
750 scanner (Epson America, Long Beach, CA). Inducible ScMed21 strains (iMed21) were grown
751 overnight, and then diluted back to 100 events per microliter as determined by flow cytometry
752 and grown at 30C with 250rpm in a deepwell 96-well plate format. Strains were supplemented
753 with β-estradiol (20μM) for 4 hours followed by Rapamycin addition. Samples were analyzed by
754 flow cytometry throughout these growth experiments.
755
756 **Western Blot**
757 Yeast cultures that had been incubated overnight in synthetic complete (SC) media were diluted
758 to OD600 = 0.6 and incubated until cultures reached OD600 ~1. Cells were harvested by
759 centrifugation. Cells were lysed by vortexing for 5 min in the presence of 200 µl of 0.5-mm
760 diameter acid washed glass beads and 200 µl SUMEB buffer (1% SDS, 8 M urea, 10 mM
761 MOPS pH 6.8, 10 mM EDTA, 0.01% bromophenol blue, 1mM PMSF) per one OD unit of original
762 culture. Lysates were then incubated at 65° for 10 min and cleared by centrifugation prior to
763 electrophoresis and blotting. Antibodies: Anti-HA-HRP (REF-12013819001, Clone 3F10,
764 Roche/Millipore Sigma, St. Louis, MO), Anti-FLAG (F3165, Monoclonal ANTI-FLAG® M2,
765 Millipore Sigma, St. Louis, MO), Anti-FRB (ALX-215-065-1, Enzo Life Sciences, Farmingdale,
766 NY, (Haruki et al., 2008)), Anti-VP16 (1-21) (sc-7545, Santa Cruz Biotechnology, Dallas TX),
767 Anti-GFP (ab290, AbCam, Cambridge, United Kingdom), Anti-MYC (71d10, 2278S, Cell
768 Signaling, Danvers, MA), Anti-PGK1 (ab113687, AbCam, Cambridge, United Kingdom).

769

770 **Protein expression and purification**

771 All multimer deficient TPL proteins were expressed in *Escherichia coli* Rosetta 2 strain. Bacteria
772 cultures were grown at 37ºC until they achieved an OD^{600}nm of 0.6-0.9. Protein expression was
773 induced with isopropyl-β-D-1-thyogalactopiranoside (IPTG) at a final concentration of 400 µM at
774 18 °C overnight. Bacteria cultures were centrifuged and the pellets were resuspended in the
775 buffer A (CAPS 200 mM pH 10.5, NaCl 500 mM, TCEP 1 mM), where cells were lysed by
776 sonication. His-tagged AtTPL188 (wt and mutants) bacteria pellets were resuspended in buffer
777 A with EDTA-free antiprotease (Roche). The soluble fractions recovered after sonication were
778 passed through a Ni-sepharose (GE Healthcare) column previously washed with buffer A and
779 the bound proteins were eluted with buffer A with 250 mM imidazole. A second purification step
780 was carried out on Gel filtration Superdex 200 10/300 GL (GE Healthcare) equilibrated with
781 buffer A.

782

783 **Co-Immunoprecipitation**

784 Co-IP from yeast was performed using the cytoSUS strains. Cultures were grown to OD600 0.5
785 (~1E7 cells/ml) using selective media, harvested, and resuspended in 200 µl SUME (1% SDS,
786 8M Urea, 10mM MOPS, pH 6.8, 10mM EDTA) buffer with protease inhibitors. Cells were lysed
787 by vortexing 3 X 1 min full speed with 100 µl of 0.5 mm Acid Washed Glass Beads, clarified by
788 centrifugation (1 min, 1000rpm), and supernatant was mixed with 1ml IP buffer (15mM
789 Na2HPO4, mw 142; 150mM NaCl, mw 58; 2% Triton X-100, 0.1% SDS, 0.5% DOC, 10mM
790 EDTA, 0.02% NaN3) with protease inhibitors, and incubated with 100 µl of IgG sepharose at
791 25°C for 2 hours with rotation. The Beads were washed 1x with IP buffer, and 2x with IP-Wash
792 buffer (50mM NaCl, mw58; 10mM TRIS, mw 121; 0.02% NaN3) with protease inhibitors. Protein
793 was eluted with 50 µl of SUME buffer + 0.005% bromophenol blue by incubation at 65°C for 10
794 minutes and run on handmade 12% acrylamide SDS-PAGE gels, and western blotted
795 accordingly. Co-IPs from tobacco were performed on leaves two days after injection as
796 described in (Song et al., 2014). For Co-IPs with HA, extracts were incubated with Anti-HA-
797 Biotin (High Affinity (3F10), Sigma, 12158167001) and Streptavidin conjugated magnetic beads
798 (). For Co-IPs with MED10B-MEC-ProtA we used IgG Sepharose® 6 Fast Flow (Sigma, GE17-
799 0969-01) beads and increased washing steps (1xIP buffer, 4xWash buffer, 5 total). The only
800 modification to buffers was an addition of the detergent NP-40 at 0.1% in the IP and wash

buffer. Samples were run on handmade 10% acrylamide SDS-PAGE gels, and western blotted accordingly.

Bimolecular Fluorescence Complementation (BiFC)

Bimolecular fluorescent complementation experiments were performed on 3-week-old *N. benthamiana* plants grown at 22°C under long days (16 h light/8 h dark) on soil (Sunshine #4 mix) as per (Martin et al., 2009). pSITE vectors were used to generate BiFC constructs for MED21, Δ5-MED21, TPL and $TPL^{H8QuadA}$ – proteins (Martin et al., 2009). In all cases the combinations are N-terminal fusions of either the nEYFP or cEYFP to the cDNA of MED21 or TPL. RFP fused Histone H2B was used as a nuclear marker (Goodin et al., 2002). Injection of Agrobacterium strains into tobacco leaves was performed as in (Goodin et al., 2002), but the OD_{600} of the Agrobacterium culture used was adjusted to 0.5. Two days after transfection, plant leaves were imaged using an epifluorescence microscope (Leica Biosystems, model: DMI 3000B).

Protein alignments

The MED21 protein sequence was were aligned to homologs using CLC Sequence Viewer 7, a tree was constructed using a Neighbor-Joining method, and bootstrap analysis performed with 10,000 replicates.

Plant growth

For synthetic repression assays in tobacco Agrobacterium-mediated transient transformation of *Nicotiana benthamiana* was performed as per (Yang et al., 2000). 5 ml cultures of Agrobacterium strains were grown overnight at 30C shaking at 220rpm, pelleted and incubated in MMA media (10 mM MgCl2, 10 mM MES pH 5.6, 100 µM acetosyringone) for 3 hours at room temperature with rotation. Strain density was normalized to an OD600 of 1 for each strain in the final mixture of strains before injection into tobacco leaves. Leaves were removed, and 8 different regions were excised using a hole punch, placed into a 96-well microtiter plate with 100µl of water. Each leaf punch was scanned in a 4x4 grid for yellow and red fluorescence using a plate scanner (Tecan Spark, Tecan Trading AG, Switzerland). Fluorescence data was quantified and plotted in R (ggplots). For *Arabidopsis thaliana* experiments using the GAL4-UAS system (Laplaze et al., 2005), J0121 was introgressed eight times into Col-0 accession from the

C24 accession, and rigorously checked to ensure root growth was comparable to Col-0 before use. UAS-TPL-IAA14^{mED} constructs were introduced to J0121 introgression lines by floral dip method (Clough and Bent, 1998). T1 seedlings were selected on 0.5X LS (Caisson Laboratories, Smithfield, UT) + 25µg/ml Hygromycin B (company) + 0.8% phytoagar (Plantmedia; Dublin, OH). Plates were stratified for 2 days, exposed to light for 6 h, and then grown in the dark for 3 d following a modification of the method of (Harrison et al., 2006). Hygromycin resistant seedlings were identified by their long hypocotyl, enlarged green leaves and long root. Transformants were transferred by hand to fresh 0.5X LS plates + 0.8% Bacto agar (Thermo Fisher Scientific) and grown vertically for 14 days at 22°C. Plates were scanned on a flatbed scanner (Epson America, Long Beach, CA) at day 14. *slr* and *med21/MED21* (WiscDsLox461-464K13) seeds were obtained from the Arabidopsis Biological Resource Center (Columbus, OH). CRISPR/CAS9 based mutations in AtMED2 were generated as described in (Wang et al., 2015). We created a novel mutation in *AtMED21* that introduces a single base-pair insertion of G at nucleotide 214 after the A of the start codon (i214G). This mutation alters the amino acid sequence starting at residue 25 and creates an early stop codon after 11 random amino acids (Supplemental Figure 6D).

Data submissions

All flow cytometry data will be deposited at https://flowrepository.org/. All plasmids will be deposited through Addgene at https://www.addgene.org/Jennifer_Nemhauser/.

Acknowledgements

We would like to thank Prof. Jef Boeke for kindly providing VEGAS adaptor and regulatory element plasmids; Dr. Jennifer Brophy and Prof. José Dinneny for kindly providing the pUBQ10:GAL4:VP16 plasmid; Dr. Natalia Petrenko and Dr. Kevin Struhl for kindly providing Mediator anchor away strains; and Prof. Grant Brown and Prof. Maitreya Dunham for advice on yeast genetics and approaches. We thank members of the Nemhauser group including Amy Lanctot, Romi Ramos, Eric Yang, and Dr. Sarah Guiziou for constructive discussions and comments on this manuscript. We also thank Morgan Hamm for the custom R script used here to analyze anchor away plates.

Author Contributions

Conceptualization: ARL, JLN; Investigation: ARL, WW, HPG, SG, SJS, MLZ, JEZ; Software: ARL, HPG; Formal Analysis: ARL, HPG; Visualization: ARL, WW, HPG, SG, SJS, MLZ, JEZ; Writing-Original Draft: ARL; Writing-Review & Editing: WW, HPG, SG, SJS, MLZ, JEZ, NZ, JLN; Supervision, Project administration, Funding Acquisition, Resources: JLN, NZ.

Declaration of Interests

The authors declare no competing interests.

Funding

National Institutes of Health (NIH): ARL, HPG, SG, SJS, JEZ, MZ & JLN R01- GM107084.

Howard Hughes Medical Institute (HHMI): ARL, SJS, JEZ, MZ & JLN - Faculty Scholar Award.

Ning Zheng is a Howard Hughes Medical Institute Investigator.

ARL is supported by the Simons Foundation through the Life Science Research Foundation.

879 **References**

880 Adams, G.E., Chandru, A., and Cowley, S.M. (2018). Co-repressor, co-activator and general
881 transcription factor: the many faces of the Sin3 histone deacetylase (HDAC) complex. Biochem.
882 J. *475*, 3921–3932.

883 Agarwal, M., Kumar, P., and Mathew, S.J. (2015). The Groucho/Transducin-like enhancer of
884 split protein family in animal development. IUBMB Life *67*, 472–481.

885 Asseck, L.Y., and Grefen, C. (2018). Detecting Interactions of Membrane Proteins: The Split-
886 Ubiquitin System. Methods Mol. Biol. Clifton NJ *1794*, 49–60.

887 Baumli, S., Hoeppner, S., and Cramer, P. (2005). A Conserved Mediator Hinge Revealed in the
888 Structure of the MED7·MED21 (Med7·Srb7) Heterodimer. J. Biol. Chem. *280*, 18171–18178.

889 Ben Keller, Justin Vrana, Abraham Miller, Garrett Newman, and Eric Klavins (2019). Aquarium:
890 The Laboratory Operating System (Zenodo).

891 Biddick, R., and Young, E.T. (2005). Yeast Mediator and its role in transcriptional regulation. C.
892 R. Biol. *328*, 773–782.

893 Bourbon, H.-M. (2008). Comparative genomics supports a deep evolutionary origin for the large,
894 four-module transcriptional mediator complex. Nucleic Acids Res. *36*, 3993–4008.

895 Brand, A.H., and Perrimon, N. (1993). Targeted gene expression as a means of altering cell
896 fates and generating dominant phenotypes. Dev. Camb. Engl. *118*, 401–415.

897 Busch, W., Miotk, A., Ariel, F.D., Zhao, Z., Forner, J., Daum, G., Suzaki, T., Schuster, C.,
898 Schultheiss, S.J., Leibfried, A., et al. (2010). Transcriptional control of a plant stem cell niche.
899 Dev. Cell *18*, 849–861.

900 Causier, B., Ashworth, M., Guo, W., and Davies, B. (2012). The TOPLESS interactome: a
901 framework for gene repression in Arabidopsis. Plant Physiol. *158*, 423–438.

902 Chen, G., and Courey, A.J. (2000). Groucho/TLE family proteins and transcriptional repression.
903 Gene *249*, 1–16.

Clough, S.J., and Bent, A.F. (1998). Floral dip: a simplified method for Agrobacterium-mediated transformation of Arabidopsis thaliana. Plant J. Cell Mol. Biol. *16*, 735–743.

Collins, J., O'Grady, K., Chen, S., and Gurley, W. (2019). The C-terminal WD40 repeats on the TOPLESS co-repressor function as a protein–protein interaction surface. Plant Mol. Biol. *100*, 47–58.

Delto, C.F., Heisler, F.F., Kuper, J., Sander, B., Kneussel, M., and Schindelin, H. (2015). The LisH motif of muskelin is crucial for oligomerization and governs intracellular localization. Struct. Lond. Engl. 1993 *23*, 364–373.

Dhawan, R., Luo, H., Foerster, A.M., Abuqamar, S., Du, H.-N., Briggs, S.D., Mittelsten Scheid, O., and Mengiste, T. (2009). HISTONE MONOUBIQUITINATION1 interacts with a subunit of the mediator complex and regulates defense against necrotrophic fungal pathogens in Arabidopsis. Plant Cell *21*, 1000–1019.

Dolan, W.L., and Chapple, C. (2017). Conservation and Divergence of Mediator Structure and Function: Insights from Plants. Plant Cell Physiol. *58*, 4–21.

Estrada, J., Wong, F., DePace, A., and Gunawardena, J. (2016). Information Integration and Energy Expenditure in Gene Regulation. Cell *166*, 234–244.

Flanagan, P.M., Kelleher, R.J., Sayre, M.H., Tschochner, H., and Kornberg, R.D. (1991). A mediator required for activation of RNA polymerase II transcription in vitro. Nature *350*, 436–438.

Flowers, E.B., Poole, R.J., Tursun, B., Bashllari, E., Pe'er, I., and Hobert, O. (2010). The Groucho ortholog UNC-37 interacts with the short Groucho-like protein LSY-22 to control developmental decisions in C. elegans. Dev. Camb. Engl. *137*, 1799–1805.

Fukaki, H., Tameda, S., Masuda, H., and Tasaka, M. (2002). Lateral root formation is blocked by a gain-of-function mutation in the SOLITARY-ROOT/IAA14 gene of Arabidopsis. Plant J. Cell Mol. Biol. *29*, 153–168.

Gaertner, B., and Zeitlinger, J. (2014). RNA polymerase II pausing during development. Development *141*, 1179–1183.

931 Gasperowicz, M., and Otto, F. (2005). Mammalian Groucho homologs: redundancy or
932 specificity? J. Cell. Biochem. *95*, 670–687.

933 Gibson, D.G., Young, L., Chuang, R.-Y., Venter, J.C., Hutchison, C.A., and Smith, H.O. (2009).
934 Enzymatic assembly of DNA molecules up to several hundred kilobases. Nat. Methods *6*, 343–
935 345.

936 Gietz, R.D., and Woods, R.A. (2002). Transformation of yeast by lithium acetate/single-stranded
937 carrier DNA/polyethylene glycol method. Methods Enzymol. *350*, 87–96.

938 Gonzalez, N., Pauwels, L., Baekelandt, A., De Milde, L., Van Leene, J., Besbrugge, N.,
939 Heyndrickx, K.S., Cuéllar Pérez, A., Durand, A.N., De Clercq, R., et al. (2015). A Repressor
940 Protein Complex Regulates Leaf Growth in Arabidopsis. Plant Cell *27*, 2273–2287.

941 Goodin, M.M., Dietzgen, R.G., Schichnes, D., Ruzin, S., and Jackson, A.O. (2002). pGD
942 vectors: versatile tools for the expression of green and red fluorescent protein fusions in
943 agroinfiltrated plant leaves. Plant J. Cell Mol. Biol. *31*, 375–383.

944 Grbavec, D., Lo, R., Liu, Y., and Stifani, S. (1998). Transducin-like Enhancer of split 2, a
945 mammalian homologue of Drosophila Groucho, acts as a transcriptional repressor, interacts
946 with Hairy/Enhancer of split proteins, and is expressed during neuronal development. Eur. J.
947 Biochem. *258*, 339–349.

948 Gromöller, A., and Lehming, N. (2000). Srb7p is a physical and physiological target of Tup1p.
949 EMBO J. *19*, 6845–6852.

950 Hallberg, M., Hu, G.-Z., Tronnersjö, S., Shaikhibrahim, Z., Balciunas, D., Björklund, S., and
951 Ronne, H. (2006). Functional and physical interactions within the middle domain of the yeast
952 mediator. Mol. Genet. Genomics MGG *276*, 197–210.

953 Haruki, H., Nishikawa, J., and Laemmli, U.K. (2008). The anchor-away technique: rapid,
954 conditional establishment of yeast mutant phenotypes. Mol. Cell *31*, 925–932.

955 Havens, K.A., Guseman, J.M., Jang, S.S., Pierre-Jerome, E., Bolten, N., Klavins, E., and
956 Nemhauser, J.L. (2012). A synthetic approach reveals extensive tunability of auxin signaling.
957 Plant Physiol. *160*, 135–142.

Ito, J., Fukaki, H., Onoda, M., Li, L., Li, C., Tasaka, M., and Furutani, M. (2016). Auxin-dependent compositional change in Mediator in ARF7- and ARF19-mediated transcription. Proc. Natl. Acad. Sci. U. S. A. *113*, 6562–6567.

Kagale, S., Links, M.G., and Rozwadowski, K. (2010). Genome-wide analysis of ethylene-responsive element binding factor-associated amphiphilic repression motif-containing transcriptional regulators in Arabidopsis. Plant Physiol. *152*, 1109–1134.

Kaul, A., Schuster, E., and Jennings, B.H. (2014). The Groucho co-repressor is primarily recruited to local target sites in active chromatin to attenuate transcription. PLoS Genet. *10*, e1004595.

Ke, J., Ma, H., Gu, X., Thelen, A., Brunzelle, J.S., Li, J., Xu, H.E., and Melcher, K. (2015). Structural basis for recognition of diverse transcriptional repressors by the TOPLESS family of corepressors. Sci. Adv. *1*, e1500107.

Khakhar, A., Leydon, A.R., Lemmex, A.C., Klavins, E., and Nemhauser, J.L. (2018). Synthetic hormone-responsive transcription factors can monitor and re-program plant development. ELife *7*.

Kim, M.H., Cooper, D.R., Oleksy, A., Devedjiev, Y., Derewenda, U., Reiner, O., Otlewski, J., and Derewenda, Z.S. (2004). The Structure of the N-Terminal Domain of the Product of the Lissencephaly Gene Lis1 and Its Functional Implications. Structure *12*, 987–998.

Kim, Y.J., Björklund, S., Li, Y., Sayre, M.H., and Kornberg, R.D. (1994). A multiprotein mediator of transcriptional activation and its interaction with the C-terminal repeat domain of RNA polymerase II. Cell *77*, 599–608.

Klepikova, A.V., Kasianov, A.S., Gerasimov, E.S., Logacheva, M.D., and Penin, A.A. (2016). A high resolution map of the Arabidopsis thaliana developmental transcriptome based on RNA-seq profiling. Plant J. *88*, 1058–1070.

Krogan, N.T., Hogan, K., and Long, J.A. (2012). APETALA2 negatively regulates multiple floral organ identity genes in Arabidopsis by recruiting the co-repressor TOPLESS and the histone deacetylase HDA19. Dev. Camb. Engl. *139*, 4180–4190.

985 Kumar, K.R.R., Blomberg, J., and Björklund, S. (2018). The MED7 subunit paralogs of Mediator
986 function redundantly in development of etiolated seedlings in Arabidopsis. Plant J. *96*, 578–594.

987 Labun, K., Montague, T.G., Krause, M., Torres Cleuren, Y.N., Tjeldnes, H., and Valen, E.
988 (2019). CHOPCHOP v3: expanding the CRISPR web toolbox beyond genome editing. Nucleic
989 Acids Res. *47*, W171–W174.

990 Laplaze, L., Parizot, B., Baker, A., Ricaud, L., Martinière, A., Auguy, F., Franche, C., Nussaume,
991 L., Bogusz, D., and Haseloff, J. (2005). GAL4-GFP enhancer trap lines for genetic manipulation
992 of lateral root development in Arabidopsis thaliana. J. Exp. Bot. *56*, 2433–2442.

993 Lee, J.E., and Golz, J.F. (2012). Diverse roles of Groucho/Tup1 co-repressors in plant growth
994 and development. Plant Signal. Behav. *7*, 86–92.

995 Lee, M., Chatterjee, S., and Struhl, K. (2000). Genetic analysis of the role of Pol II holoenzyme
996 components in repression by the Cyc8-Tup1 corepressor in yeast. Genetics *155*, 1535–1542.

997 Liu, Z., and Karmarkar, V. (2008). Groucho/Tup1 family co-repressors in plant development.
998 Trends Plant Sci. *13*, 137–144.

999 Liu, X., Galli, M., Camehl, I., and Gallavotti, A. (2019). RAMOSA1 ENHANCER LOCUS2-
1000 Mediated Transcriptional Repression Regulates Vegetative and Reproductive Architecture.
1001 Plant Physiol. *179*, 348–363.

1002 Long, J.A., Ohno, C., Smith, Z.R., and Meyerowitz, E.M. (2006). TOPLESS regulates apical
1003 embryonic fate in Arabidopsis. Science *312*, 1520–1523.

1004 Ma, H., Duan, J., Ke, J., He, Y., Gu, X., Xu, T.-H., Yu, H., Wang, Y., Brunzelle, J.S., Jiang, Y., et
1005 al. (2017). A D53 repression motif induces oligomerization of TOPLESS corepressors and
1006 promotes assembly of a corepressor-nucleosome complex. Sci. Adv. *3*, e1601217.

1007 Maji, S., Dahiya, P., Waseem, M., Dwivedi, N., Bhat, D.S., Dar, T.H., and Thakur, J.K. (2019).
1008 Interaction map of Arabidopsis Mediator complex expounding its topology. Nucleic Acids Res.
1009 *47*, 3904–3920.

1010 Malik, N., Agarwal, P., and Tyagi, A. (2017). Emerging functions of multi-protein complex
1011 Mediator with special emphasis on plants. Crit. Rev. Biochem. Mol. Biol. *52*, 475–502.

1012 Martin, K., Kopperud, K., Chakrabarty, R., Banerjee, R., Brooks, R., and Goodin, M.M. (2009).
1013 Transient expression in Nicotiana benthamiana fluorescent marker lines provides enhanced
1014 definition of protein localization, movement and interactions in planta. Plant J. Cell Mol. Biol. *59*,
1015 150–162.

1016 Martin-Arevalillo, R., Nanao, M.H., Larrieu, A., Vinos-Poyo, T., Mast, D., Galvan-Ampudia, C.,
1017 Brunoud, G., Vernoux, T., Dumas, R., and Parcy, F. (2017). Structure of the Arabidopsis
1018 TOPLESS corepressor provides insight into the evolution of transcriptional repression. Proc.
1019 Natl. Acad. Sci. U. S. A.

1020 Matsumura, H., Kusaka, N., Nakamura, T., Tanaka, N., Sagegami, K., Uegaki, K., Inoue, T., and
1021 Mukai, Y. (2012). Crystal structure of the N-terminal domain of the yeast general corepressor
1022 Tup1p and its functional implications. J. Biol. Chem. *287*, 26528–26538.

1023 McIsaac, R.S., Oakes, B.L., Wang, X., Dummit, K.A., Botstein, D., and Noyes, M.B. (2013).
1024 Synthetic gene expression perturbation systems with rapid, tunable, single-gene specificity in
1025 yeast. Nucleic Acids Res. *41*, e57.

1026 Mitchell, L.A., Chuang, J., Agmon, N., Khunsriraksakul, C., Phillips, N.A., Cai, Y., Truong, D.M.,
1027 Veerakumar, A., Wang, Y., Mayorga, M., et al. (2015). Versatile genetic assembly system
1028 (VEGAS) to assemble pathways for expression in S. cerevisiae. Nucleic Acids Res. *43*, 6620–
1029 6630.

1030 Mottis, A., Mouchiroud, L., and Auwerx, J. (2013). Emerging roles of the corepressors NCoR1
1031 and SMRT in homeostasis. Genes Dev. *27*, 819–835.

1032 Oberoi, J., Fairall, L., Watson, P.J., Yang, J.-C., Czimmerer, Z., Kampmann, T., Goult, B.T.,
1033 Greenwood, J.A., Gooch, J.T., Kallenberger, B.C., et al. (2011). Structural basis for the
1034 assembly of the SMRT/NCoR core transcriptional repression machinery. Nat. Struct. Mol. Biol.
1035 *18*, 177–184.

1036 Papamichos-Chronakis, M., Conlan, R.S., Gounalaki, N., Copf, T., and Tzamarias, D. (2000).
1037 Hrs1/Med3 is a Cyc8-Tup1 corepressor target in the RNA polymerase II holoenzyme. J. Biol.
1038 Chem. *275*, 8397–8403.

1039 Perissi, V., Jepsen, K., Glass, C.K., and Rosenfeld, M.G. (2010). Deconstructing repression:
1040 evolving models of co-repressor action. Nat. Rev. Genet. *11*, 109–123.

1041 Petrenko, N., Jin, Y., Wong, K.H., and Struhl, K. (2017). Evidence that Mediator is essential for
1042 Pol II transcription, but is not a required component of the preinitiation complex in vivo. ELife *6*,
1043 e28447.

1044 Pierre-Jerome, E., Jang, S.S., Havens, K.A., Nemhauser, J.L., and Klavins, E. (2014).
1045 Recapitulation of the forward nuclear auxin response pathway in yeast. Proc. Natl. Acad. Sci. U.
1046 S. A. *111*, 9407–9412.

1047 Pierre-Jerome, E., Wright, R.C., and Nemhauser, J.L. (2017). Characterizing Auxin Response
1048 Circuits in Saccharomyces cerevisiae by Flow Cytometry. Methods Mol. Biol. Clifton NJ *1497*,
1049 271–281.

1050 Raya-González, J., Ortiz-Castro, R., Ruíz-Herrera, L.F., Kazan, K., and López-Bucio, J. (2014).
1051 PHYTOCHROME AND FLOWERING TIME1/MEDIATOR25 Regulates Lateral Root Formation
1052 via Auxin Signaling in Arabidopsis. Plant Physiol. *165*, 880–894.

1053 Raya-González, J., Oropeza-Aburto, A., López-Bucio, J.S., Guevara-García, Á.A., de Veylder,
1054 L., López-Bucio, J., and Herrera-Estrella, L. (2018). MEDIATOR18 influences Arabidopsis root
1055 architecture, represses auxin signaling and is a critical factor for cell viability in root meristems.
1056 Plant J. Cell Mol. Biol. *96*, 895–909.

1057 Samanta, S., and Thakur, J.K. (2015). Importance of Mediator complex in the regulation and
1058 integration of diverse signaling pathways in plants. Front. Plant Sci. *6*, 757.

1059 Sato, S., Tomomori-Sato, C., Tsai, K.-L., Yu, X., Sardiu, M., Saraf, A., Washburn, M.P., Florens,
1060 L., Asturias, F.J., Conaway, R.C., et al. (2016). Role for the MED21-MED7 Hinge in Assembly of
1061 the Mediator-RNA Polymerase II Holoenzyme. J. Biol. Chem. *291*, 26886–26898.

1062 Schreiber-Agus, N., Chin, L., Chen, K., Torres, R., Rao, G., Guida, P., Skoultchi, A.I., and
1063 DePinho, R.A. (1995). An amino-terminal domain of Mxi1 mediates anti-Myc oncogenic activity
1064 and interacts with a homolog of the yeast transcriptional repressor SIN3. Cell *80*, 777–786.

1065 Siligato, R., Wang, X., Yadav, S.R., Lehesranta, S., Ma, G., Ursache, R., Sevilem, I., Zhang, J.,
1066 Gorte, M., Prasad, K., et al. (2016). MultiSite Gateway-Compatible Cell Type-Specific Gene-
1067 Inducible System for Plants. Plant Physiol. *170*, 627–641.

1068 Song, Y.H., Estrada, D.A., Johnson, R.S., Kim, S.K., Lee, S.Y., MacCoss, M.J., and Imaizumi,
1069 T. (2014). Distinct roles of FKF1, GIGANTEA, and ZEITLUPE proteins in the regulation of
1070 CONSTANS stability in Arabidopsis photoperiodic flowering. Proc. Natl. Acad. Sci. *111*, 17672–
1071 17677.

1072 Sood, V., Cajigas, I., D'Urso, A., Light, W.H., and Brickner, J.H. (2017). Epigenetic
1073 Transcriptional Memory of GAL Genes Depends on Growth in Glucose and the Tup1
1074 Transcription Factor in Saccharomyces cerevisiae. Genetics *206*, 1895–1907.

1075 Ulmasov, T., Hagen, G., and Guilfoyle, T.J. (1997). ARF1, a transcription factor that binds to
1076 auxin response elements. Science *276*, 1865–1868.

1077 Wang, Z.-P., Xing, H.-L., Dong, L., Zhang, H.-Y., Han, C.-Y., Wang, X.-C., and Chen, Q.-J.
1078 (2015). Egg cell-specific promoter-controlled CRISPR/Cas9 efficiently generates homozygous
1079 mutants for multiple target genes in Arabidopsis in a single generation. Genome Biol. *16*, 144.

1080 Weber, E., Engler, C., Gruetzner, R., Werner, S., and Marillonnet, S. (2011). A Modular Cloning
1081 System for Standardized Assembly of Multigene Constructs. PLOS ONE *6*, e16765.

1082 Wong, K.H., and Struhl, K. (2011). The Cyc8-Tup1 complex inhibits transcription primarily by
1083 masking the activation domain of the recruiting protein. Genes Dev. *25*, 2525–2539.

1084 Wong, M.M., Guo, C., and Zhang, J. (2014). Nuclear receptor corepressor complexes in cancer:
1085 mechanism, function and regulation. Am. J. Clin. Exp. Urol. *2*, 169–187.

1086 Wright, R.C., Bolten, N., and Pierre-Jerome, E. (2019). flowTime: Annotation and analysis of
1087 biological dynamical systems using flow cytometry (Bioconductor version: Release (3.10)).

Yang, Y., Li, R., and Qi, M. (2000). In vivo analysis of plant promoters and transcription factors by agroinfiltration of tobacco leaves. Plant J. *22*, 543–551.

Zhang, Z., and Reese, J.C. (2004). Redundant Mechanisms Are Used by Ssn6-Tup1 in Repressing Chromosomal Gene Transcription in Saccharomyces cerevisiae. J. Biol. Chem. *279*, 39240–39250.

Zhang, Y., Gao, S., and Wang, Z. (2010). Structural and functional analysis of amino-terminal enhancer of split in androgen-receptor-driven transcription. Biochem. J. *427*, 499–511.

Zhu, J., Jeong, J.C., Zhu, Y., Sokolchik, I., Miyazaki, S., Zhu, J.-K., Hasegawa, P.M., Bohnert, H.J., Shi, H., Yun, D.-J., et al. (2008). Involvement of Arabidopsis HOS15 in histone deacetylation and cold tolerance. Proc. Natl. Acad. Sci. *105*, 4945–4950.

Zhu, J., Liu, M., Liu, X., and Dong, Z. (2018). RNA polymerase II activity revealed by GRO-seq and pNET-seq in Arabidopsis. Nat. Plants *4*, 1112–1123.

Supplemental Figures

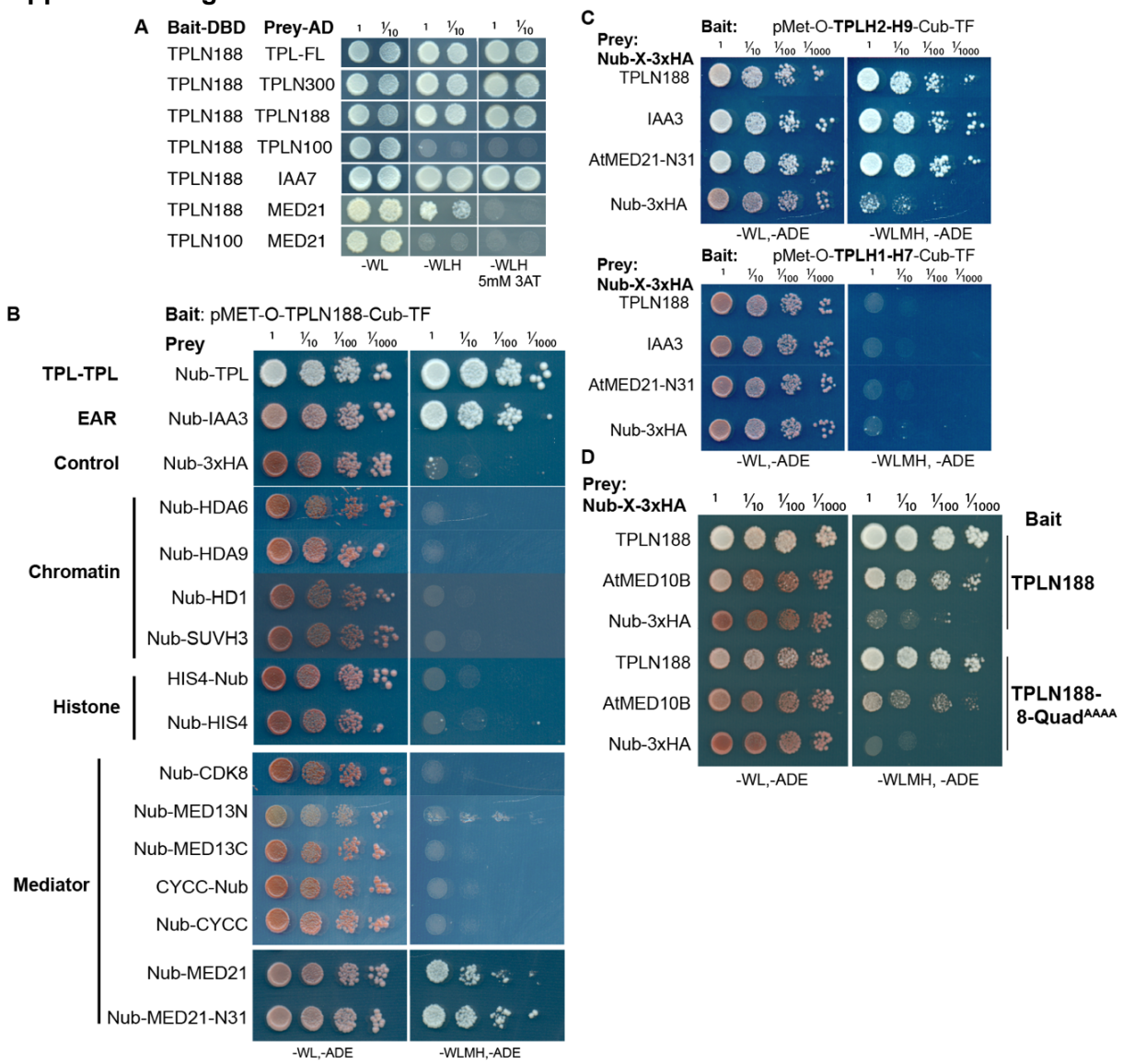

Supplemental Figure 1. The TPL-N terminal domain (TPLN188) interacts with the N-terminus of AtMED21. **A.** Identifying TPL-N terminal domain interactor proteins through Yeast Two Hybrid screening identifies TPL as a problematic Bait protein, as it may silence the activation despite successful binding of a prey protein (see second row from bottom where N188 and MED21 show very weak reporter activity on 3AT). 3AT - 3-Amino-1,2,4-triazole. Plates were measured after 3 days to allow TPL-MED21 interactions to grow. **B.** Identifying TPL-N terminal domain interactor proteins through cytoplasmic split ubiquitin protein interaction assay. We tested the N-terminal and C-terminal portions of MED13 separately and divided the coding sequence at amino acid 967 (MED13N = aa1-967, MED13C = aa968-1908). Each bait tested is the *Arabidopsis* homolog cloned from cDNA from the Col-0 accession, with the

exception of *AtMED13*, which was synthesized *de novo* via Twist (https://www.twistbioscience.com/). Plates were scanned at 3 days after plating to allow weaker interactions to develop if they were present. **C.** TPL interacts with MED21 through an interaction within Helices 8-9. Plates were scanned at 2 days after plating. **D.** The Helix 8 Quadruple mutation (V145A, E146A, K148A, K149A) does not affect AtMED10B binding to TPL. Plates were scanned at 3 days after plating. **B-D.** The relative position of the N-terminal portion of ubiquitin (Nub) is indicated for each bait protein.

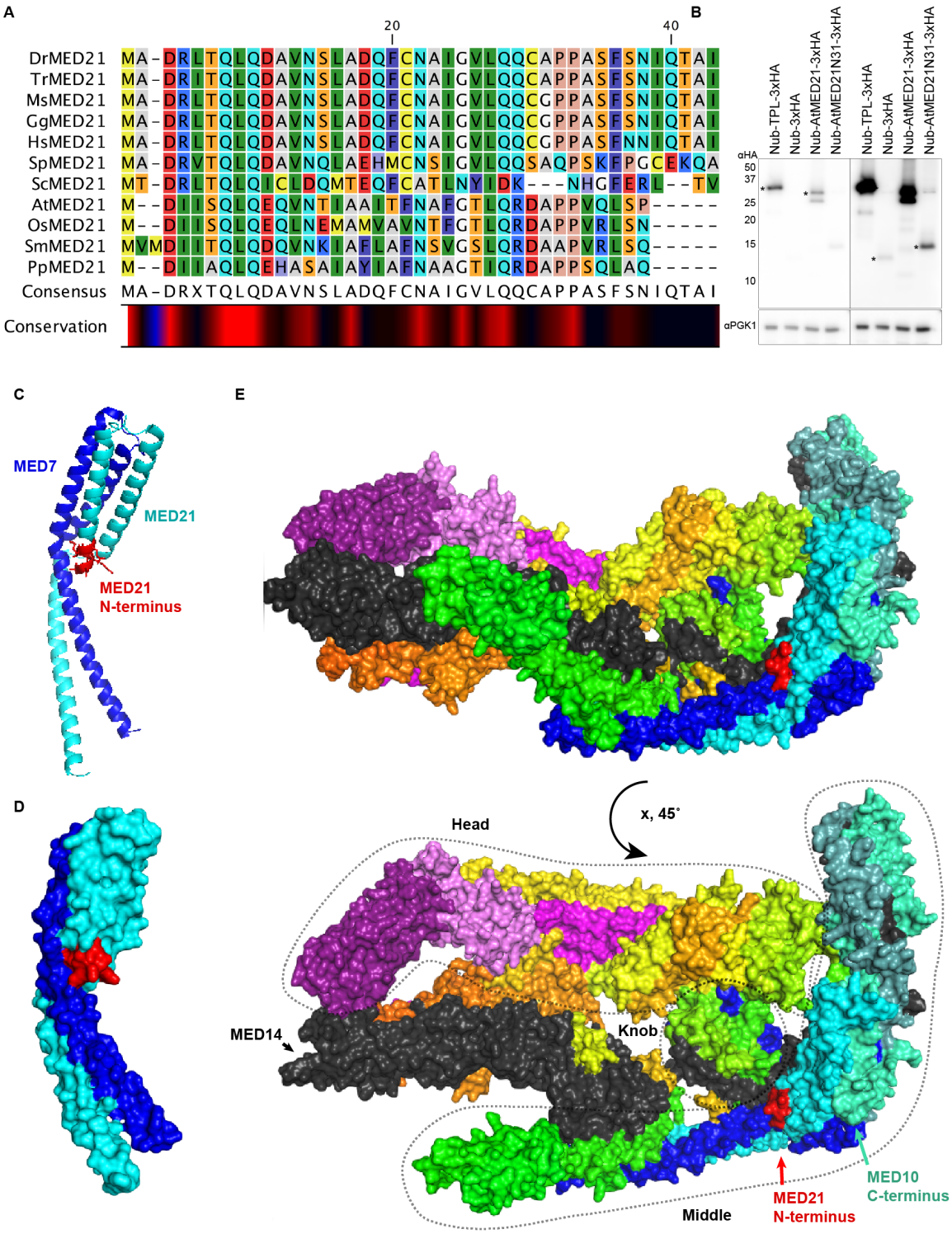

Supplemental Figure 2. Homology and structure of the MED21 subunit of the mediator complex. A. Protein levels of AtMED21 cytoSUS constructs in yeast. Two different exposure times are shown to demonstrate the lower abundance of the truncation with only the first 31

amino acids of the AtMED21 (N31). Asterisks indicate the size predicted for the indicated protein. **B.** Protein alignment of selected MED21 homologs from various species. Dr - *Drosophila melanogaster*, Tr - *Takifugu rubripes*, Ms - *Mus musculus*, Gg - *Gallus gallus*, Hs - *Homo sapiens*, Sp - *Strongylocentrotus purpuratus*, Sc - *Saccharomyces cerevisiae*, At - *Arabidopsis thaliana*, Os - *Oryza sativa*, Sm - *Selaginella moellendorffii*, Pp - *Physcomitrella patens*. Alignment was performed in CLC sequence viewer 7, using a neighbor joining method. **C-D.** Structure of the MED21 (Cyan) & MED7 (Blue) hetero dimer, adapted from 1YKH, (Baumli et al., 2005). The amino acids in the N-terminus that were solved are highlighted in red up to the 7th amino acid of the yeast MED21. **C.** The cartoon visualization, **D.** Surface visualization. **E.** Core mediator (5N9J, (Nozawa et al., 2017)) with the location of MED21 and MED7 indicated with the same colors from (C-D). In this structure the location of the MED21 N-terminus is again indicated in red, demonstrating its close proximity to the Knob region (dotted circle).

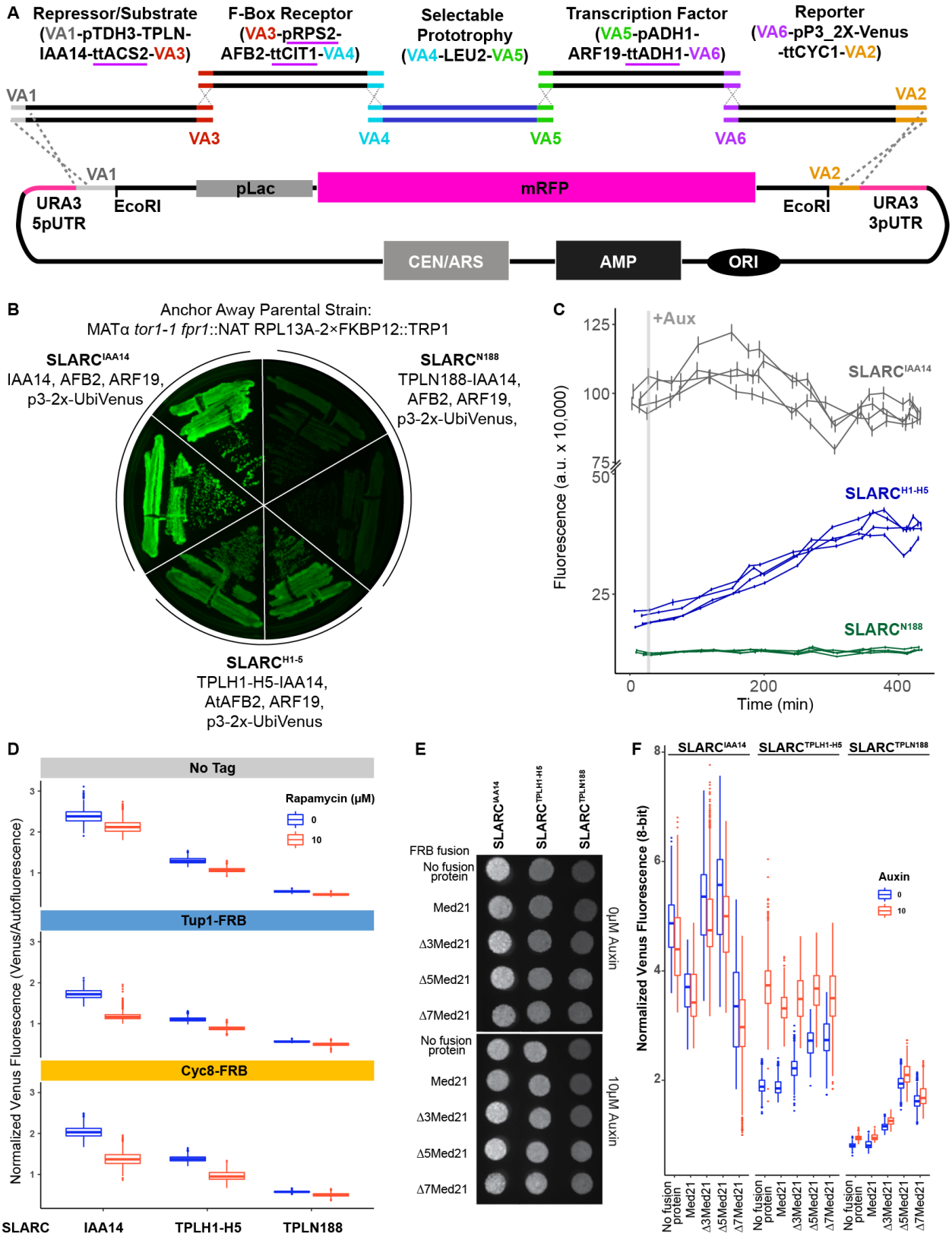

Supplemental Figure 3. Construction and characterization of the Single Locus Auxin Response Circuit (SLARC). A. Design schematic of the approach utilized to create the SLARC through a VEGAS assembly approach. Each individual transcriptional unit (TU) was checked to replace promoters or terminators that utilized identical sequences and replaced with an alternative sequence indicated by a purple underline. These TUs were assembled into level 1 plasmids by Golden Gate reaction. Subsequently, they were amplified by PCR using primers specific for the Vegas Adaptor (VA) sequences specific for their TU cassette. In example, for the first Repressor/Substrate TU the TU was amplified using primers for VA1 and VA3 and purified by a PCR cleanup column (NEB). The acceptor plasmid was cut with EcoRI and both TU and acceptor plasmid was transformed into yeast and recombinant plasmids were selected on synthetic drop out (SDO) plates lacking Leucine. **B.** Primary SLARC transformants were struck out onto fresh SDO -Leu and imaged for Venus expression, demonstrating varying levels of reporter expression that correlate with TPL repressor domains. Plasmid DNA was purified from these strains and sequenced to confirm the proper recombination of TU cassettes. **C.** Time course flow cytometry of SLARC strains following auxin addition. For all cytometry experiments, the indicated TPL construct is fused to IAA14, because this IAA works better in haploid yeast strains that IAA3. Every point represents the average fluorescence of 5-10,000 individually measured yeast cells (a.u. - arbitrary units). Auxin (IAA-10μM) was added at the indicated time (gray bar, + Aux). Four independent experiments are shown for each construct. **D.** The yeast TPL homolog Tup1 and its partner protein Cyc8 do not repress the SLARC. Quantified fluorescence from the single locus auxin response circuit (SLARC) introduced into Tup1 and Cyc8 anchor away lines demonstrates no increased fluorescence from the reporter upon depletion of Tup1 or Cyc8 from the nucleus. Anchor away depletion of Tup1 or Cyc8 results in slower yeast growth. To normalize for this disparity in growth, Venus fluorescence was normalized to red autofluorescence, where each pixel was normalized to the corresponding red autofluorescence collected for that position and plotted as a boxplot. Two individual biological replicates (two separate experiments) were evaluated, and the data was pooled. **E-F.** Med21 N terminal deletions are viable in *Saccharomyces* and demonstrate altered SLARC transcriptional states. **E.** A representative grayscale image of fellow fluorescence of spot plates of yeast strains carrying SLARC plasmids in Med21 N-terminal deletions. Each is plated at an OD600 of 0.1 on SDO with or without auxin (10μM IAA). **F.** Venus fluorescence from (**E**) was normalized to red background (autofluorescence), where each pixel was normalized to the corresponding red

1173 autofluorescence collected for that position and plotted as a boxplot. Two individual biological
1174 replicates (two separate experiments) were evaluated, and the data was pooled and is
1175 presented as boxplots.
1176

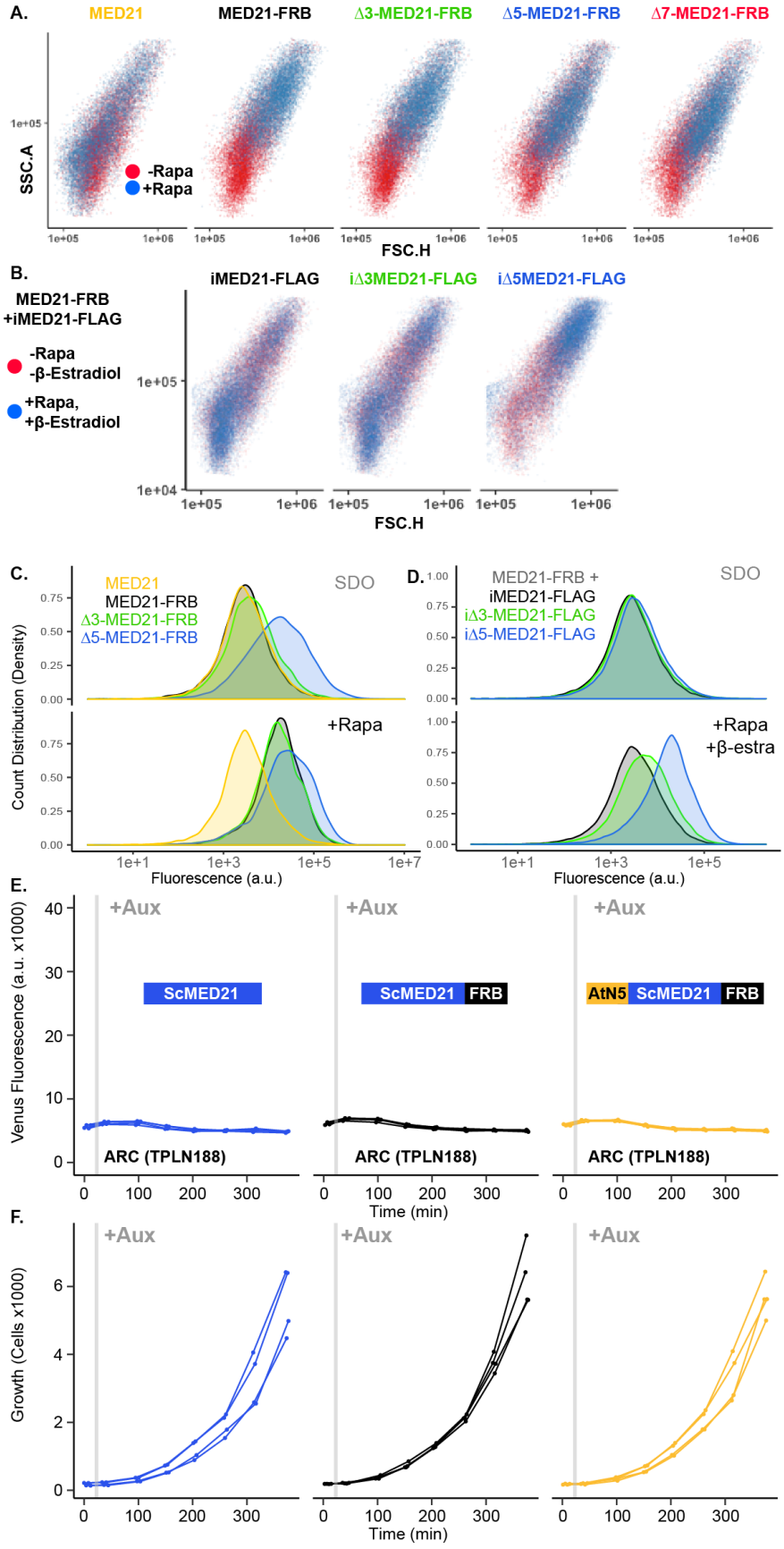

Supplemental Figure 4. Inducible MED21 rescues rapamycin induced yeast growth defects. A. Depletion of nuclear ScMed21 by Rapamycin increased cell size even in short time-courses, consistent with its essential role in many core pathways. Scatterplots of side scatter area by forward scatter height (SSC.A x FSC.H) indicate large scale increases in cell size in populations of yeast with (blue) or without (red) Rapamycin treatment. **B.** Inducible Med21 (iMed21) wild type and variants cell size were examined before (red) and after (blue) treatment with Rapamycin and b-estradiol to simultaneously deplete the wild-type Med21-FRB fusion, and induce the transcription of the Med21 variant. Scatterplots of side scatter area by forward scatter height (SSC.A x FSC.H) demonstrate a less disrupted cell size compared to Anchor Away strains in (**A**). **C-D.** Histograms of Venus fluorescence in inducible Med21 (iMed21) strains demonstrate that populations were evenly distributed around a single mean, suggesting we were observing the immediate effects of the Med21 deletions. The histograms were built using ggplots Density function to create a visualization of count distribution. These samples were tested at 300 minutes (as in Figure 4D), and plotted to visualize cells at the equivalent stage of growth, Med21 depletion, and induction. **C.** Effect of anchor away of Med21-FRB variants alone and **D.** Depletion of ScMed21-FRB after induction (b-estradiol added 4 hours before Rapamycin treatment) of iMed21. **E**. Conversion of the first five amino acids of ScMed21 to the corresponding sequence from AtMED21 results in an identical repression profile. Time course flow cytometry of SLARC strains following auxin addition. For all cytometry experiments, the indicated TPL construct is fused to IAA14, because this IAA performs better in haploid yeast strains that IAA3. Every point represents the average fluorescence of 5-10,000 individually measured yeast cells (a.u. - arbitrary units). Auxin (IAA-10μM) was added at the indicated time (gray bar, + Aux). Two independent experiments are shown for each construct. **F.** Cell growth of the strains in (**E**) indicate the swap of the N-terminal region had no effect on yeast growth or viability. Data presented is events per microliter over the time-course of the cytometry experiments. **C.** Protein expression analysis by western blotting of strains used in A & B. In this ARC, TPLN188-IAA3 is N-terminally fused to 2xHA. Total protein loading levels were tested by blotting against the housekeeping gene PGK1 (bottom panel).

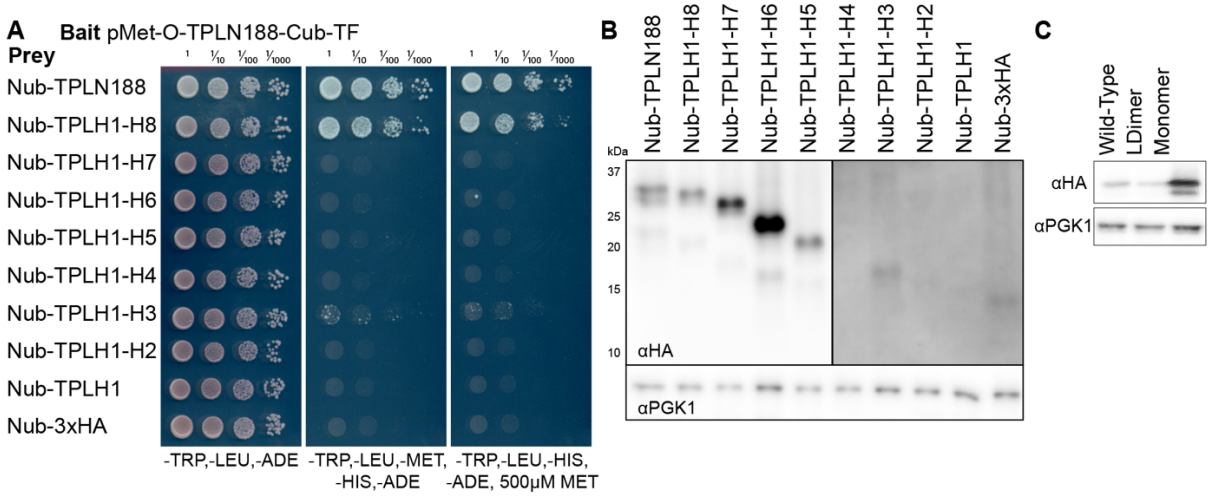

Supplemental Figure 5. TPL multimerization requires Helix 8. A. Cytoplasmic split ubiquitin interaction (cytoSUS) assay on serial deletions of TPL. Interaction of bait and prey proteins reconstitute split ubiquitin, release a synthetic transcription factor that allows growth on media lacking Histidine and Adenine. The expression level of the bait protein can be repressed through increased Methionine in the media. **B**. Protein levels of Nub-TPL fusions were tested by PAGE and western blotting for the c-terminal 3xHA epitope tag included in all constructs. Deletions longer than H1-4 are detectable at higher levels (left panel), whereas shorter isoforms required longer exposure times to detect (right panel). Total protein loading levels were tested by the housekeeping gene PGK1 (bottom panel). **C.** Protein expression analysis by western blotting of tetramerization mutants expressed in yeast for cytoSUS interaction assay in Figure 5I. Prey constructs are C-terminally fused to 2xHA. Total protein loading levels were tested by blotting against the housekeeping gene PGK1 (bottom panel).

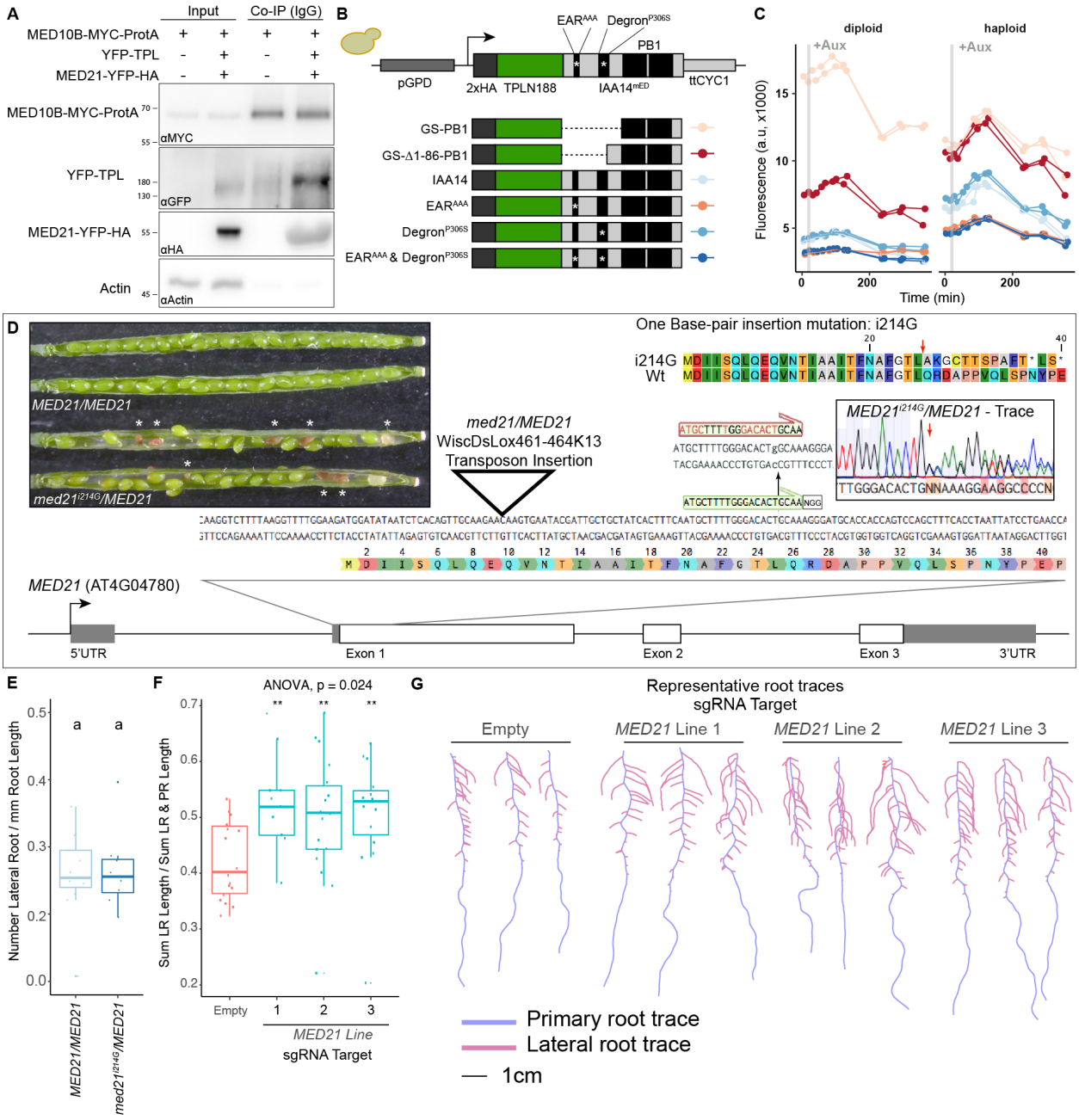

Supplemental Figure 6. The TPL-MED21 interaction is required for repression in plants. **A.** MED21 and TPL Co-Immunoprecipitated with AtMED10B from tobacco extracts. Each construct was expressed under the viral 35S promoter, and tissues were harvested after 2 days of injection. MED10B was purified by incubation with IgG sepharose beads (see methods), and the presence of interacting proteins was determined by western blotting. Actin was used as a control to determine the efficacy of washing. **B-C.** Engineering and prototyping a variant of TPLN-IAA14^{mED} which carries mutations in the EAR domain (EAR^{AAA}) and in the degron (P306S) in yeast. **B.** Cartoon schematic of the mutations tested during prototyping of the

TPLN188-IAA14mED construct. In each case the identical glycine-serine linker (GS) was used as the flexible linker between the 2xHA-TPLN188 protein and the portion of IAA14 retained in the construct. **C.** Time course flow cytometry of TPLN-IAA14^{mED} strains following auxin addition. Strains containing the TPLN-IAA14^{mED} was tested in both haploid and diploid strains and demonstrated similar repression profiles. Every point represents the average fluorescence of 5-10,000 individually measured yeast cells (a.u. - arbitrary units). Auxin (IAA-10μM) was added at the indicated time (gray bar, + Aux). Two independent experiments are shown for each construct. **D.** Identification and characterization of a novel CAS9-based insertional mutation in *MED21*. The *MED21* genomic locus (AT4G04780) is shown as a cartoon, with a zoom in on the beginning of the coding sequence highlighted with the amino acid sequence. The location of the *med21/MED21* mutant (WiscDsLox461-464K13, see triangle), and the sgRNA we employed (see green annotation and NGG PAM site) highlighted. The insertion of a G at nucleotide position +214 after the transcriptional start site abrogates the sgRNA site (red annotation above with i214G). A representative sequencing trace demonstrates the position where the heterozygote carries i215G, and the predicted effect to the coding sequence is shown at the top right – a red arrow indicates the first codon affected by the i214G mutation. The Inset pictures at the top left demonstrate the embryo lethality phenotype in *med21*^{i214G}*/MED21* heterozygote siliques. White asterisks indicate the embryos that have begun to degenerate. These aborted seeds are visibly brown indicating that fertilization took place allowing the seed coat to form before development failed. **E.** *med21*/*MED21* heterozygotes are haplo-sufficient for lateral root development. Lateral root density (number of lateral roots / primary root length) was calculated at 10 days post germination. Lower case letters indicate significant difference (ANOVA and Tukey HSD multiple comparison test; $p<0.001$). **F.** Ratio of lateral root lengths to total root lengths (lateral root lengths + primary root length) in dCAS9 repressor lines targeting *MED21* calculated at 10 days post germination. Statistical tests (ANOVA and Wilcox test) are reported above the graph. **G.** Representative root traces of dCAS9 repressor lines targeting *MED21* calculated at 10 days post germination.